INTERNAL FLOW SUBJECTED TO AN AXIAL VARIATION OF THE EXTERNAL HEAT TRANSFER COEFFICIENT

by

James H. Beale

Thesis submitted to the Faculty of the Virginia Polytechnic Institute and State University in partial fulfillment of the requirements for the degree of

Master of Science

in

Mechanical Engineering

APPROVED:

Dr. Brian Vick, Chairman

Dr. D. J. Nelson

Dr. R. T. Smith

April 1987

Blacksburg, Virginia

INTERNAL FLOW SUBJECTED TO AN AXIAL VARIATION OF THE EXTERNAL HEAT TRANSFER COEFFICIENT

by

James H. Beale

ABSTRACT

A theoretical investigation of internal flow subjected to an axial variation of the external convection coefficient is presented. Since the variable boundary condition parameter causes the problem to become nonseparable, conventional techniques do not apply. Instead, the Green's function technique is used to convert the governing partial differential equations into a singular Volterra integral equation for the temperature of the fluid at the wall. The integral equation is resolved numerically by the trapezoid rule with the aid of a singularity subtraction procedure. The solution methodology is developed in terms of a fully turbulent flow which is shown to contain fully laminar and slug flow as special cases.

Before examining the results generated by numerical solution of the integral equation, a thorough study is made of each of the building blocks required in the solution procedure. A comparison of the respective dimensionless velocity profiles and dimensionless total

diffusivities for each of the flow models is presented. Next, an analysis of the eigenvalue problem for each flow model is presented with consideration given to the normalized eigenfunctions and the eigenvalues themselves. Finally, the singular nature of the Green's function is examined showing the effect of the parameters Ho, Re and Pr.

The technique is applied to study the heat transfer from a finned tube. A parameter study is presented to examine the effects of the external finning and the flow model. The effect of external finning is examined through specific variations of the external convection coefficient, while the flow model is selected through the velocity profile and eddy diffusivity. In examining turbulent flow, the effects of the parameters, Re and Pr, are considered.

ACKNOWLEDGEMENTS

It is indeed a pleasure to acknowledge the members of my Advisory Committee: Chairman Dr. Brian Vick, Dr. Douglas Nelson and Dr. Robert Smith. Very special gratitude is extended to Dr. Brian Vick for guiding me through the perils of graduate study with seemingly endless patience. I would also like to thank the National Science Foundation for providing research funding through grant number MEA-8403964. My parents deserve a heartfelt thanks for providing support and motivation throughout my life and especially during the past year. Also, I would like to thank Gina for providing support and sufficient distraction to enable me to maintain my sanity.

TABLE OF CONTENTS

LIST OF FIGURES

LIST OF FIGURES (continued)

LIST OF TABLES

NOMENCLATURE

A	polynomial spline function, defined in Table 1, row 3
$A_{c,b}$	fin base area
b	polynomial spline function, defined in Table 1, row 4
C_f	friction factor
C_p	specific heat
F	polynomial spline function, defined in Table 1, row 2
$f(\xi)$	function defined by Eq. (23c)
$g(\eta)$	dimensionless total diffusivity
G	Green's function
$\overline{G}$	transformed Green's function
$h(z)$	external heat transfer coefficient
$H(\xi)$	dimensionless heat transfer coefficient
H_o	constant heat transfer coefficient
i	geometry specifier
$J_p(\eta)$	Bessel function of order p
k	thermal conductivity
K	kernel defined by Eq. (23b)
N_m	normalization integral
Nu	Nusself number
P	pressure
Pe	Peclet number
Pr	Prandtl number
Pr_t	turbulent Prandtl number
q	heat transfer rate
$Q(\xi)$	dimensionless heat transfer rate

NOMENCLATURE (continued)

r	radial variable
r_o	tube radius
Re	Reynolds number
Re*	Reynolds number based on u*, Re $\sqrt{C_f/2}$
$S(\eta,\xi)$	dimensionless heat source
$T(r,z)$	mean temperature
T_o	inlet temperature
T_∞	ambient temperature
T'	fluctuating temperature
$u(r)$	mean velocity profile
u'	fluctuating axial velocity
u^*	friction velocity, $\sqrt{\tau_\omega/\rho}$
u^+	dimensionless velocity, $u(r)/u^*$
u_b	bulk velocity
$v(\eta)$	dimensionless velocity, $u(r)/u_b$
v'	fluctuating radial velocity
y_i^+	polynomial spline function, defined in Table 1, row 1
z	axial variable

Greek Symbols

α	thermal diffusivity
δ	delta function
ε_f	fin efficiency
ε_H	eddy diffusivity
ε_m	eddy viscosity
η	dimensionless radial variable

NOMENCLATURE (continued)

η_i	$1 - 2y_i^+/Re^*$
$\theta(\eta,\xi)$	dimensionless temperature
$\theta_b(\xi)$	dimensionless bulk temperature
$\theta_w(\xi)$	dimensionless wall temperature
λ_m	mth eigenvalue
ν	kinematic viscosity
ξ	dimensionless axial variable
ρ	density
σ	small positive quantity
τ_w	wall shear stress
$\psi_m(\eta)$	mth normalized eigenfunction

I. INTRODUCTION

This work describes a theoretical investigation of the effect of an axially varying external convection coefficient on the heat transfer characteristics in fully developed internal flow. The solution methodology is presented in terms of a fully developed turbulent flow, for either a parallel plate geometry or a smooth round tube and an arbitrary axial variation of the external convection coefficient. The results are applicable to laminar and slug flow in either geometry since these two cases can be considered as special cases of the more complex turbulent flow situation.

In general, the solution of a convective heat transfer problem requires the separate solution of the appropriate governing equations for the flow field and the temperature field. The solution of the momentum equations for slug or laminar flow in either geometry presents no particular difficulty. However, in the case of a fully developed turbulent duct flow no exact solution to the momentum equations is possible due to the complex, three dimensional and random flow field. Therefore, recourse must be made to a turbulence model in which some empirical information is necessarily included. After an extensive literature review, the turbulence model of Travis, Buhr and Sesonske [1] was selected as the most accurate available for the fully turbulent flow of a fluid in a smooth pipe, since it satisfies all known analytical constraints and agrees with the best available experimental data.

Once a complete description of the velocity distribution is available, it is possible to attempt the solution of the thermal energy equation. However, the effect of the variable boundary condition param-

eter is to render the governing thermal energy equation nonseparable and as a consequence, all standard analytical techniques such as the finite integral transform technique or Green's functions fail. This is why such an important problem with many practical applications remains relatively untouched.

By employing a variable external convection coefficient or variable Biot number, it is possible to model many situations of engineering interest. Perhaps the most striking example of an engineering situation that can be modeled by a variable Biot number is the effect of external finning on the heat transfer to an internal flow. Each fin can be considered as a heat transfer device that increases the local heat transfer from the fin base, at temperature T_b, to the ambient, at temperature T_∞. By employing the fin effectiveness, ε_f, defined as the ratio of the heat transfer from the fin to the heat transfer that would exist in the same area without the fin, it is possible to write the amount of heat transferred to the surroundings from the fin as

$$q_f = \varepsilon_f h_1 A_{c,b}(T_b - T_\infty) \tag{1}$$

where h_1 is the external heat transfer coefficient along the unfinned section of the duct and $A_{c,b}$ is the cross-sectional area of the fin at the base. By defining a fin heat transfer coefficient as $h_2 = \varepsilon_f h_1$, it is possible to model a duct fitted with an array of external fins as an unfinned duct with a stepwise periodic variation of the external convection coefficient. Another model for the Biot number variation arises through a consideration of axial conduction in the duct wall. Since

wall conduction should have a smoothing effect on the abrupt changes in the external convection coefficient, a harmonic variation of the Biot number is also considered. A schematic of the externally finned duct and the variations of the external convection coefficient are presented in Fig. 1.

There are numerous applications in engineering where external fins are important, such as in industrial and residential heating equipment, power plant heat exchange equipment and radiators for internal combustion engines. Other applications for which a variable convection coefficient could be used include cryogenic refrigeration systems, shell and tube heat exchangers, and nuclear fuel elements. In the past, these systems have been designed from experience, experimental data and limited one dimensional analytical studies. In some applications, such as the design of heat exchangers for use in space vehicles, it is necessary to accurately predict the heat transfer characteristics, so that the system can meet size and weight restrictions. For this reason, it is necessary to have theoretical models available so that many designs can be considered as efficiently as possible in the optimization process.

In spite of the numerous applications, there are no works in the literature examining turbulent flow with a variable external heat transfer coefficient. A few studies have been conducted on heat transfer to laminar pipe flow with a variable convective boundary. Sparrow and Charmchi [2] used a finite difference scheme to solve the Graetz problem for a stepwise periodic variation of the heat transfer coefficient. However, the discontinuous nature of the boundary condition made the

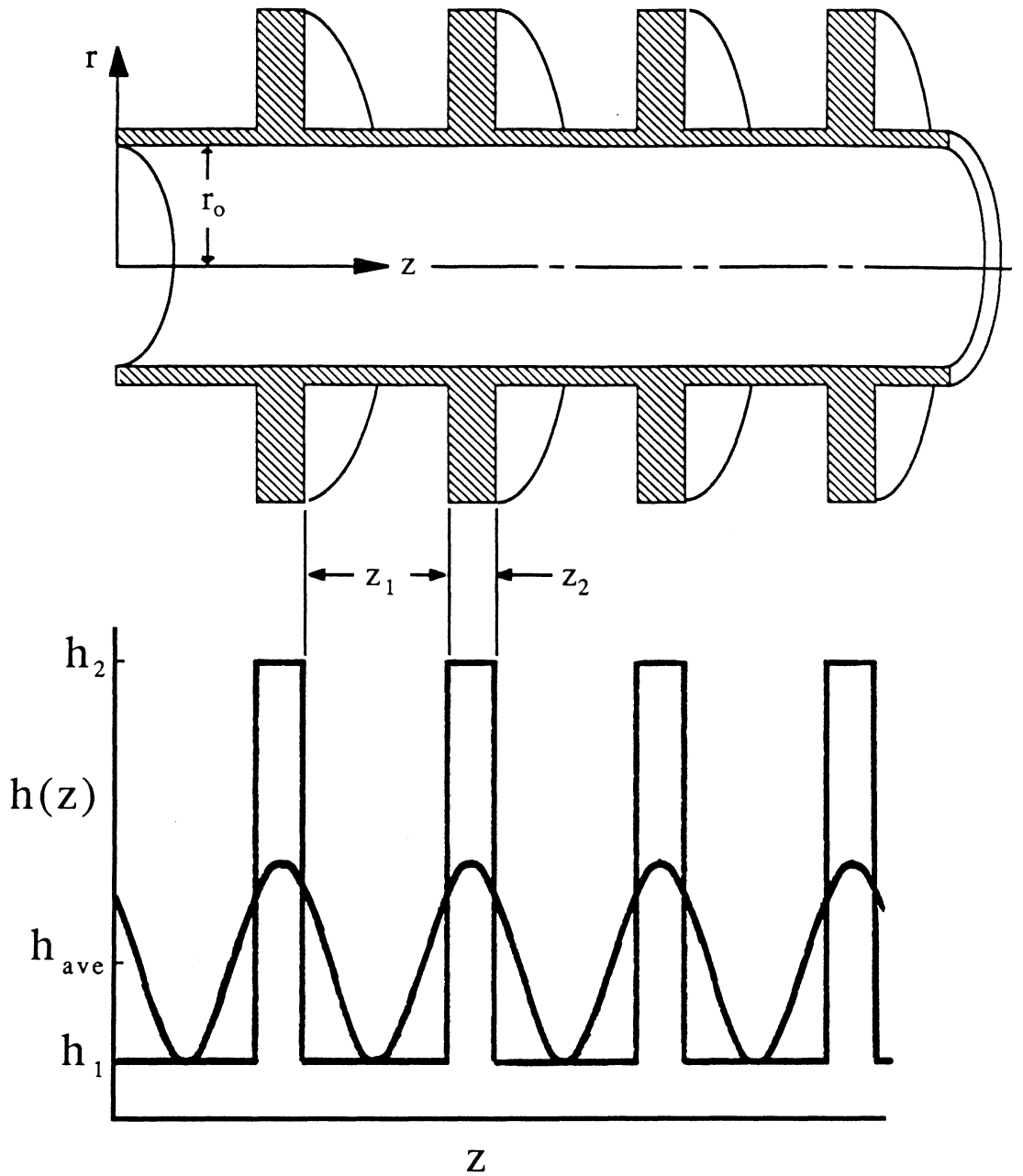

Figure 1. (a) Externally finned tube, (b) Convection coefficient variations

computational task quite demanding, so that a complete parameter study was not possible. The only analytical study of the problem was performed by Vick and Wells [3], in which they used a variable eigenvalue technique to study laminar flow with an axially varying heat transfer coefficient. The technique requires a separate analysis for each variation of the convection coefficient and would be quite demanding for the case of a harmonic variation.

The present investigation presents a solution methodology for heat transfer to a fully developed internal duct flow subjected to an arbitrary axial variation of the external heat transfer coefficient. The standard Green's function method is used to convert the governing thermal energy equation and boundary conditions into a singular Volterra integral equation for the temperature of the fluid at the wall. The integral equation is then resolved with a standard numerical integration procedure. Results are presented for slug, laminar and turbulent flow in a round tube for both stepwise and harmonic variations of the Biot number.

II. LITERATURE REVIEW

A. Internal Flow Heat Transfer

There have been numerous investigations into internal flow heat transfer dating from the original Graetz investigation in 1885 [4]. Since then, the work of Graetz has been extended to cover a wide range of physical situations, including slug, laminar, turbulent and non-Newtonian flow in ducts of arbitrary cross-section. In these works, attention is focused on boundary conditions of the first, second and third kinds, or, the specified wall temperature, the specified wall heat flux and the convective boundary condition, respectively. The majority of the investigations deal with the boundary conditions of the first and second kind. An authoritative review of the works published in this area before 1978 is included in Shah and London [5].

The solution to the problem of slug flow with negligible axial conduction is well known for each of the three boundary conditions. The results for this problem can be found in many heat transfer texts.

The problem of heat transfer to a fully-developed laminar flow is slightly more difficult than the slug flow case because the resulting eigenvalue problem is more complicated. Nevertheless, a great deal of research has been accomplished in this area. Siegel, et al [6] use a method of superposition to handle an arbitrary axial distribution of the wall heat flux. Hsu [7] applied Duhamel's theorem to solve the energy equation with a harmonic variation of the wall heat flux. Mitchell [8] used a polynomial approximation to describe a specified variation of the wall temperature and then applied Duhamel's theorem. Shapovalov [9]

utilized an expansion in terms of the hypergeometric function for an arbitrary heat flux variation. Zaychik [10] used a Laplace transform technique to solve the Graetz problem. Other methods used to solve the Graetz problem include the Monte Carlo technique [11] and the finite element method [12]. Casarella, et al. [13] used the method of conformal mapping to extend the solution of laminar pipe flow to a duct of arbitrary cross section. Problems involving viscous dissipation and thermal energy generation have been solved by the Laplace transform technique [14] and the variational method [15].

In the study of heat transfer to a fully-developed turbulent flow, the solution is complicated by the lack of an analytical expression for the velocity distribution. The standard means of overcoming this difficulty lies in time-averaging the governing momentum equation, however, this introduces an extra unknown into the system of equations resulting in the well-known closure problem of turbulence. Thus, it is necessary to include some empirical information in the formulation.

Although there has been a great deal of work simply modelling the experimental velocity distributions, the eddy viscosity derived from such a velocity profile is not very accurate since the eddy viscosity depends on the radial derivative of the velocity profile. The introduction of the eddy viscosity concept is due to Boussinesq [16], who proposed that a constant value for the eddy viscosity be used. However, the eddy viscosity is not a property of the fluid only and hence is not constant. Prandtl [17] introduced the idea of a mixing length which is still used even though it is based on an erroneous physical concept. Deissler [18] extended Prandtl's idea to include an

exponential decay wall damping term based on an exact analysis of the oscillating plate problem. Riechardt [19] devised an eddy viscosity relationship in two regions, the wall section and the core section, which fit the experimental data very well. The velocity profile obtained from an integration of his eddy viscosity was able to match the velocity profile in both the wall and core regions very well. Recently, Travis, Buhr and Sesonske [1] have modified Reichardt's two region model to produce an eddy viscosity and velocity profile which satisfy all known analytical constraints and satisfy the best available experimental data. Since reference [1] provides the best available turbulence model, it is used in this investigation.

The problem of heat transfer to a turbulent stream has received considerable attention in the literature. Martinelli [20] studied the case of constant wall temperature for heat transfer to the turbulent flow of a molten metal. Sleicher and Tribus [21] solved the case of a step change in wall temperature and showed how this solution can be extended to solve the cases of an arbitrary wall temperature variation and a uniform wall heat flux. In a three paper exposition, Notter et al. [22,23,24] used the method of matched asymptotic expansions to solve the turbulent Graetz problem for the cases of uniform wall temperature and uniform wall heat flux. Shibani and Ozisik [25] considered the turbulent flow between parallel plates using the matched asymptotic expansion technique. In each of these investigations, relatively simple expressions for the eddy diffusivity and velocity profiles were used to accommodate the mathematical technique. There do not appear to be any investigations concerning the effect of a convective boundary condition on the heat transfer to a turbulent pipe flow.

B. Augmented Heat Transfer

There are several techniques available to designers for enhancing the rate of heat transfer from an internal flow. Among these are extended surfaces, twisted tape inserts, vibration of the tube, electrostatic fields and fluid additives [26,27].

The most common means of increasing the rate of heat transfer from an internal flow is through external finning. However, the exact analysis of a fin assembly is extremely complicated because the heat flow is three dimensional and is coupled with both the internal and external fluid motion. To simplify the analysis, a set of classical assumptions attributed to Gardner [28] is applied. These assumptions state that the heat flow in the fin is steady and one-dimensional. Harper and Brown [29] introduced the idea of analyzing an individual fin apart from the supporting surface. This allows a nondimensional representation of the heat transfer rate from the fin, the fin efficiency, to be calculated from a small number of fin parameters. Gardner [28] presents fin efficiency curves for many different types of fin including straight fins, annular fins and spines. The fin efficiencies provide a simple means of modelling a finned duct as an unfinned duct subjected to an overall heat transfer coefficient, which is derived from a one dimensional analysis of the finned and unfinned sections

Much of the recent work on external fins involves the optimization of individual fins. Razelos [30] maximized the heat transfer from a pin fin while minimizing the fin volume. Kovarak [31] maximized the heat transfer from straight fins while minimizing cost. Razelos and Imre [32] obtained optimum dimensions of a circular fin of trapezoidal

profile including the effects of a variable thermal conductivity and a variable convection coefficient. Other optimization criteria include a minimization of entropy production in fins by Poulikakos and Bejan [33], and a least weight circular fin by Guceri [34].

Nowhere in the literature was a combined analysis of duct and fin assembly coupled with the internal flow problem considered. This is due to the difficulty inherent in such an analysis and the difficulty in presenting data in compact form.

C. Variable Boundary Condition Parameters

This investigation deals with the heat transfer to an internal flow by virtue of an axial variation of the heat transfer coefficient. In general, though, the problem belongs to the broader class of problems dealing with variable boundary condition parameters. The work done in this area is not extensive, due to the mathematical complexity involved with variable boundary condition parameters. Investigations have focused on transient heat conduction, periodic contact analysis, and phase change. There are two works concerning the effect of an axial variation of the heat transfer coefficient on laminar pipe flow.

Mikhailov [35] presents a general solution to the heat equation with a time dependent convection coefficient using time dependent eigenvalues to overcome the nonseparable condition inherent in such problems. Ozisik and Murray [36] apply a variable eigenvalue approach to analyze linear diffusion problems with both time and space dependent coefficients. Ivanov and Salomatov [37] introduce a change of variables in the heat conduction equation to eliminate the variable parameter in

the boundary condition. Unfortunately, the change of variables introduces a nonlinear term into the heat conduction equation. Thompson and Holy [38] present an analysis of the quenching of a sphere subjected to a time-dependent heat transfer coefficient using Volterra integral equations. Holy [39] extended this work to consider time and space dependent heat transfer coefficients in nuclear reactor fuel elements. In reference [39] a variety of methods are considered to solve for the temperature and thermal stress distribution in both a sphere and a thick slab subjected to spatially and time varying heat transfer coefficients.

Periodic contact analysis involves heat transfer across solids which are brought into contact and then separated in a continuous cycle. Reed and Mullineux [40] examined the quasi-steady state temperature distribution within a cylinder in periodic contact with a surface by the use of a semi-numerical procedure. Mikhailov [41] addressing the same problem, applied a finite integral transform technique to reduce the solution to a system of simultaneous algebraic equations for the temperature transform. Vick and Ozisik [42] examined the problem of two finite periodically contacting regions with convective heat loss during separation and an imperfect thermal contact at the interface. They used the finite integral transform technique to reduce the problem to a system of algebraic equations for the transformed temperatures.

In phase change problems, the location of the phase change front varies with time, creating a nonseparable condition, since the location of the front is not known a priori. Ozisik and Guceri [43] adopt a variable eigenvalue approach to solve the phase change problem in a slab. They formally devise an infinite set of coupled ordinary

differential equations, but adopt the zeroth order solution, meaning they neglect all but the first of these equations.

The effect of an axial variation of the external heat transfer coefficient on a laminar pipe flow is considered by Sparrow and Charmchi [2]. The investigation employs the definition of the fin effectiveness to model the externally finned tube as an unfinned tube subjected to an axial variation of the heat transfer coefficient. A finite difference scheme is employed which, due to the rapidly changing nature of the boundary condition, required between ten and twenty million grid points. Therefore, a full parameter study was not feasible. In a recent work, Vick and Wells [3] employed a variable eigenvalue approach to study the problem considered in reference [2]. The variable eigenvalue approach has the advantage of being a completely analytical solution to the problem, with the only drawback being that the details of the solution become excessively complicated for variations of the convection coefficient other than stepwise periodic.

D. Mathematical Theory

The general theory of nonsingular second order Volterra integral equations was developed around the turn of the century by Volterra. The classical theory as well as the more recent functional analytic approach are presented in a few good books [44,45].

In general, however, integral equations with singular kernels are very difficult to handle. The theory behind singular Volterra integral equations is still under development. Some basic results of existence and uniqueness are presented in Hochstadt [44]. On a more practical

level Brunner [47] presents a survey of recent advances in the numerical treatment of Volterra integral and integro-differential equations. In reviewing the methods used to handle equations with a weakly singular kernel, he indicates that a theory of direct quadrature or Runge-Kutta-type methods does not yet exist. He reports that most of the work done has concentrated on developing collocation methods in conjuction with the product integration technique to discretize the resulting integral expressions. Brunner and te Riele [48] present methods with arbitrary orders of convergence for the approximate solution of second kind Volterra integral equations with weakly singular kernels. The methods are based on collocation techniques in certain nonsmooth piecewise function spaces whose elements reflect the singular behavior of the given equation. Bownds [49] combines a kernel approximation technique involving Chebyshev expansions with a recursive collocation in the space of piecewise continuous polynomials to solve a certain class of singular Volterra integral equations. Linz [50] presents a method of numerical integration of singular Volterra integral equations based on the method of product integration, which involves approximation of the kernel by a linear combination of simple basis fuctions, chosen such that the resulting integrals can be computed analytically. Garey [51] considers the numerical solution of singular Volterra integral equations that may be nonlinear. He generalizes the product integration technique used in reference [50] and develops the results in terms of a numerical quadrature of arbitrary order. Bownds and Wood [52] use a modified Galerkin method to obtain solutions to a singular, possibly nonlinear Volterra integral equation with monotonic kernels. te Riele [53] uses a

collocation method to study weakly singular Volterra integral equations of the second kind. El Tom [54] develops an excellent solution technique for second-order singular Volterra integral equations using spline functions. With this technique, approximate solutions of arbitrarily high order can be developed easily.

In this investigation, a Volterra integral equation of the second kind with a weakly singular kernel is developed for the case of heat transfer to an internal flow by virtue of an axial variation of the convection coefficient. The solution of the integral equation is developed in terms of a singularity subtraction procedure which apparently has not been previously applied to equations of Volterra type. The technique of singularity subtraction is well known, however, and has been applied to singular Fredholm integral equations by Kleinman [61] in the study of scattering theory. A general discussion of singularity subtraction can be found in Delves and Mohamed [64].

In the next section, the equations governing the flow field and the temperature field are presented.

III. FORMULATION

The system under investigation consists of a fully developed internal flow which enters an uninsulated section of duct at the origin of coordinates. It is assumed that the flow has passed through a sufficient length of insulated duct to become hydraulically fully developed and to achieve a uniform temperature profile, $T(r,0) = T_o$. The flow itself is Newtonian with constant properties and may be either laminar or turbulent. At the origin of coordinates, the flow begins to exchange heat with its surroundings, at temperature T_∞, by virtue of an axial variation of the heat transfer coefficient, $h(z)$. A schematic of the situation is shown in Fig. 2.

Since knowledge of the velocity distribution in the duct is a prerequisite for a solution of the thermal energy equation, the formulation of the equations governing the flow field precedes the formulation of the equations governing the temperature field. In both cases, the formulation is presented in terms of an arbitrary, fully-developed turbulent flow in either a flat plate or tube geometry. The equations for laminar flow can then be immediately obtained as a special case of the more general turbulent case.

A. Flow Field

Since the velocity field in turbulent flow is random, three dimensional and unsteady, an exact mathematical description of the process is impossible at present. The usual way to proceed involves expressing the dependent variables in the Navier-Stokes equations as the sum of mean and fluctating quantities and then time averaging [55]. The resulting axial momentum equation is

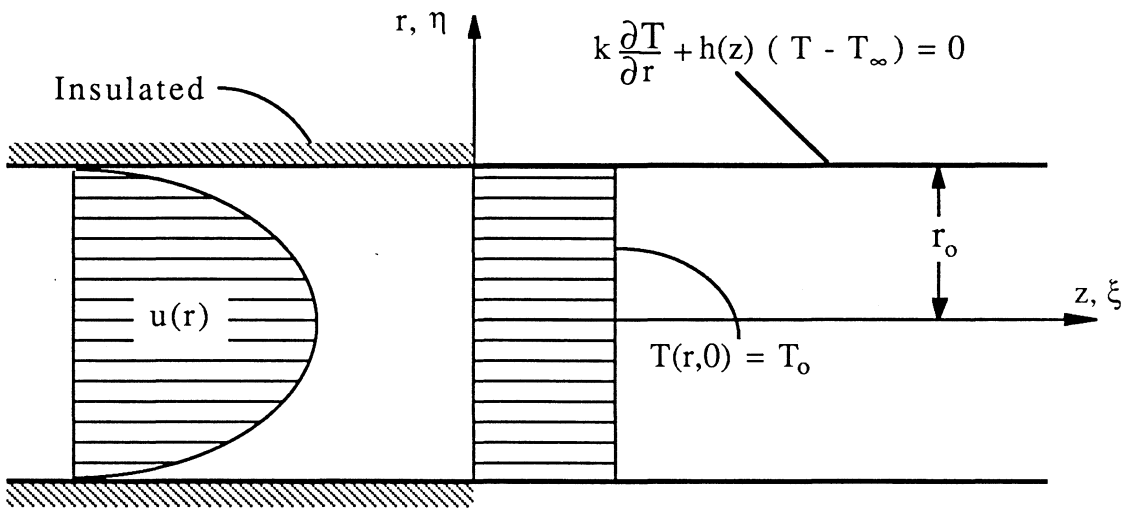

Figure 2. Geometry and coordinates

$$\frac{1}{\rho}\frac{dP}{dz} = \nu \frac{1}{r^i}\frac{d}{dr}\left(r^i \frac{du}{dr}\right) - \frac{1}{r^i}\frac{d}{dr}\left(r^i \overline{u'v'}\right) \tag{2}$$

The contribution of the turbulence has survived in the term, $\overline{u'v'}$ where the overbar denotes a time-averaged term. Boussinesq [16] was the first to introduce the eddy viscosity concept, with which the term $\overline{u'v'}$ is expressed in terms of the mean velocity gradient as follows,

$$\overline{u'v'} = -\varepsilon_m \frac{du}{dr} \tag{3}$$

where ε_m is the eddy viscosity. Using this relation, equation (2) can be rewritten in a form similar to that of laminar flow,

$$\frac{1}{\rho}\frac{dP}{dz} = \frac{1}{r^i}\frac{d}{dr}\left[r^i \left(\nu + \varepsilon_m\right)\frac{du}{dr}\right] \tag{4a}$$

Appropriate boundary conditions are,

$$\frac{du}{dr} = 0 \quad , \quad r = 0 \tag{4b}$$

$$u = 0 \quad , \quad r = r_o \tag{4c}$$

$$\varepsilon_m = 0 \quad , \quad r = r_o \tag{4d}$$

The geometry specifier, i, permits the choice of either the parallel plate or the tube coordinate system, as follows,

$$i = \begin{cases} 0 \quad , & \text{parallel plate} \\ 1 \quad , & \text{tube} \end{cases} \tag{5}$$

Equation (4a) can be integrated for the three special cases of slug, laminar and turbulent flows. For slug flow, both the viscosity and the eddy viscosity are zero. Also, the boundary condition (4c) can no longer be enforced. The trivial result is

$$u(r) = u_b \tag{6}$$

where

$$u_b = \frac{2}{r_o^{i+1}} \int_{r=o}^{r_o} r^i u(r) dr$$

For laminar flow the eddy viscosity is zero and the governing equation (4a) can be directly integrated to yield the well-known parabolic velocity profile [65]. In terms of the bulk velocity this is

$$u(r) = \begin{cases} \frac{3}{2} u_b \left[1 - \left(\frac{r}{r_o}\right)^2 \right] & , \quad \text{parallel plate} \\ 2u_b \left[1 - \left(\frac{r}{r_o}\right)^2 \right] & , \quad \text{tube} \end{cases} \tag{7}$$

For turbulent flow, the eddy viscosity is a function of r, so that integration of Eq. (4a) yields

$$\frac{1}{\rho} \frac{r}{2^i} \frac{dP}{dz} = (\nu + \varepsilon_m) \frac{du}{dr} \tag{8}$$

The pressure gradient is related to the friction velocity, u^*, by an overall force balance as follows,

$$\frac{1}{\rho}\frac{dP}{dz} = -\frac{2^i}{r_o}u^{*2} \tag{9}$$

so that (8) becomes

$$\frac{r}{r_o}u^{*2} = -(\nu + \varepsilon_m)\frac{du}{dr} \tag{10}$$

Note that Eq. (10) has the same form for both geometries since i does appear explicitly. This can be integrated in terms of the still unknown eddy viscosity to yield the velocity profile for turbulent flow,

$$u(r) = \frac{u^{*2}}{r_o}\int_r^{r_o}\frac{rdr}{(\nu + \varepsilon_M)} \tag{11}$$

In the analysis section, the turbulence model of Travis, Buhr and Sesonske [1] is used to determine the appropriate form for the eddy viscosity, ε_m.

Now that the velocity profiles have been established, the form of the governing energy equation will be presented.

B. Temperature Field

The form of the governing energy equation for a turbulent flow is obtained with an identical procedure to the one used to derive the time averaged momentum equation. The result is

$$\rho c_p u(r)\frac{\partial T}{\partial z} = \frac{k}{r^i}\frac{\partial}{\partial r}\left(r^i\frac{\partial T}{\partial r}\right) - \frac{\rho c_p}{r^i}\frac{\partial}{\partial r}\left(r^i\overline{v'T'}\right) + s(r,z) \tag{12}$$

Here, the term $\rho c_p \overline{v'T'}$ is modeled as a turbulent heat flux in the form

$$\overline{v'T'} = - \varepsilon_H \frac{\partial T}{\partial r} \tag{13}$$

so that Eq. (12) can be rewritten as

$$\rho c_p u(r) \frac{\partial T}{\partial z} = \frac{1}{r^i} \frac{\partial}{\partial r} \left[r^i \left(k + \rho c_p \varepsilon_H \right) \frac{\partial T}{\partial r} \right] + s(r,z) \tag{14a}$$

The necessary boundary conditions are taken as,

$$\frac{\partial T}{\partial r} = 0 \tag{14b}$$

$$k \frac{\partial T}{\partial r} + h(z)(T - T_\infty) = 0 \quad , \quad r = r_o \tag{14c}$$

$$T = T_o \quad , \quad z = 0 \tag{14d}$$

A turbulent Prandtl number can be defined as

$$Pr_t = \frac{\varepsilon_m}{\varepsilon_H}$$

Since the mechanisms for turbulent transport of heat and momentum are postulated to be the same, Pr_t is taken as a constant. There is some disagreement regarding the most appropriate value for Pr_t since it actually varies slightly across the flow channel and depends on the thermal boundary condition at the wall [56]. However, a constant value of $Pr_t = 0.9$ has been found to correlate well with experimental data and is used here.

Introducing the following dimensionless variables, equations (6), (7), (11) and (14) can be written in a more convenient form,

$$\eta = \frac{r}{r_o} \quad , \quad \xi = \frac{z}{(r_o P_e)} \tag{15a,b}$$

$$Re = \frac{2 r_o u_b}{\nu} \quad , \quad Pr = \frac{\nu}{\alpha} \quad , \quad Pe = Re\ Pr \tag{15c,d,e}$$

$$v(\eta) = \frac{u(r)}{u_b} \quad , \quad g(\eta) = 1 + \frac{Pr}{Pr_t} \frac{\varepsilon_m}{\nu} \tag{15f,g}$$

$$H(\xi) = \frac{h(z) r_o}{k} \quad , \quad S(\eta,\xi) = \frac{r_o^2\, s(r,z)}{k(T_o - T_\infty)} \tag{15h,i}$$

$$\theta(\eta,\xi) = \frac{T(r,z) - T_\infty}{T_o - T_\infty} \tag{15j}$$

The equations for the velocity profile in dimensionless form can be summarized as follows,

$$v(\eta) = \begin{cases} 1 \quad , \quad \text{slug flow} & (16a) \\ \frac{3}{2}(1 - \eta^2) \quad , \quad \text{laminar flow in parallel plate} & (16b) \\ 2(1 - \eta^2) \quad , \quad \text{laminar flow in tube} & (16c) \\ \frac{1}{2} \frac{Re^{*2}}{Re} \int_\eta^1 \frac{\eta\, d\eta}{\left(\frac{\varepsilon_m}{\nu} + 1\right)} \quad , \quad \text{turbulent flow} & (16d) \end{cases}$$

The dimensionless energy equation with boundary conditions is written,

$$\frac{v(\eta)}{2}\frac{\partial\theta}{\partial\xi} = \frac{1}{\eta^i}\frac{\partial}{\partial\eta}\left[\eta^i g(\eta)\frac{\partial\theta}{\partial\eta}\right] + S(\eta,\xi) \qquad (17a)$$

$$\frac{\partial\theta}{\partial\eta} = 0 \quad , \quad \eta = 0 \qquad (17b)$$

$$\frac{\partial\theta}{\partial\eta} + H(\xi)\theta = 0 \quad , \quad \eta = 1 \qquad (17c)$$

$$\theta = 1 \quad , \quad \xi = 0 \qquad (17d)$$

This set of equations models the thermal entry region in a duct with a fully developed flow entering at a uniform temperature, T_o. The fluid exchanges heat with its surroundings by virture of an axially varying heat transfer coefficient, h(z). The fully developed flow may be chosen as either inviscid, laminar or turbulent by using the appropriate form of the velocity and eddy diffusivity profiles, $v(\eta)$ and $g(\eta)$, respectively. A choice of geometry is provided through the geometry specifier, i, given by Eq. (5). A source term is included to allow for heat generation or viscous dissipation.

The main interest with this set of equations is the boundary condition at $\eta = 1$. The parameter $H(\xi)$ allows for the modelling of various situations of engineering interest such as the effect of external finning or the effect of an external flow which cools the duct and varies in the axial direction. The main difficulty with a variable boundary condition parameter is that it renders the governing energy

equation nonseparable so that standard analytical techniques cannot be used. In the next section, a straightforward method for handling an arbitrary variation of $H(\xi)$ is developed.

IV. ANALYSIS

A. Flow Field

In the turbulence model of Travis, Buhr and Sesonske [1], Reichardt's two region eddy viscosity model [19] is modified so that the eddy viscosity and the resulting velocity profile satisfy the following constraints:

i) The eddy viscosity must vanish with the cube of the distance from the wall.

ii) The eddy viscosity must be a smooth function of radial position.

iii) The velocity gradient must vanish at the pipe center.

iv) The continuity equation must be satisfied by the mean velocity.

v) Values of the wall shear stress should follow the accepted friction factor vs. Reynolds number relationship.

vi) Point values of the velocity should agree with the best available experimental data.

vii) The predicted ratio of bulk velocity to maximum velocity should fit the experimental data.

The modified Reichardt equations are, for the wall region,

$$\left(\frac{\varepsilon_m}{\nu}\right)_w = b\left[y^+ - A \tanh\left(\frac{y^+}{A}\right)\right] \quad , \quad y < y_i^+ \tag{18a}$$

and, for the central region

$$\left(\frac{\varepsilon_m}{\nu}\right)_c = \frac{b}{6}\frac{Re^*}{2}\left[1 - (Fn)^2\right]\left[\frac{2}{3} + 2(Fn)^2\right] \quad , \quad n \leq n_i \tag{18b}$$

where

$$y^+ = \frac{Re^*}{2}(1 - n)$$

Using the seven constraints outlined above, the problem is reduced to the solution of four simultaneous non-linear equations for the four unknown functions, b, A, F and y_i^+ or η_i. The solution was carried out in reference [1], and the four functions of Re are presented in a table of polynomial spline functions, reproduced here for convenience as Table 1. The value of each function, b, A, F and y_i^+ represented by $\phi(Re)$ is given by

$$\phi(Re) = \sum_{j=0}^{3} a_j(\log Re - \alpha)^j$$

over the range

$$\alpha \leq (\log Re) \leq \beta$$

The description of the turbulence is now complete, with relations for the eddy viscosity available from Eqs. (18a,b) and the table of polynomial spline functions in Table 1. The time-averaged turbulent velocity profile is obtained through numerical integration of Eq. (16d).

B. Temperature Field

The system of equations (17) for the developing temperature profile is now solved by employing the Green's function technique to convert the original partial differential equation and boundary conditions into a singular Volterra integral equation for the temperature of the fluid at

Table 1. Polynomial spline functions eddy diffusivity model[+]

	α	β	a_0	a_1	a_2	a_3
$\phi(Re) = y_i^+$	3.602	3.888	24.91	-12.580	22.780	-21.350
	3.888	5.805	22.68	-4.791	4.489	-0.623
	5.805	6.700	25.60	5.546	0.903	-1.851
$\phi(Re) = F$	3.602	3.931	1.123	-0.3755	0.6173	-0.4733
	3.931	4.421	1.049	-0.1230	0.1501	-0.0798
	4.421	5.129	1.015	-0.0334	0.0329	-0.0132
	5.129	6.700	1.004	-0.0066	0.0049	-0.0013
$\phi(Re) = A$	3.602	3.950	19.77	-19.19	26.91	-19.47
	3.950	4.787	15.52	-7.533	6.565	-1.655
	4.787	5.884	12.84	-0.046	2.387	-0.598
	5.884	6.700	14.87	3.031	0.417	-1.116
$\phi(Re) = 100b$	3.602	4.643	52.34	-7.276	4.034	-0.123
	4.643	4.767	49.00	0.728	3.652	-3.447
	4.767	6.700	49.14	1.472	2.375	-0.945

[+]Table reproduced from reference [1].

the wall.

A Green's function is chosen which is governed by the following system of equations,

$$\frac{v(\eta)}{2}\frac{\partial G}{\partial \xi} = \frac{1}{\eta^i}\frac{\partial}{\partial \eta}\left[\eta^i g(\eta)\frac{\partial G}{\partial \eta}\right] + \delta^i(\eta - \eta_o)\delta(\xi - \xi_o) \tag{19a}$$

$$\begin{aligned} &\frac{\partial G}{\partial \eta} = 0 \quad , \quad \eta = 0 \ (i = 0) \\ &G,\ \frac{\partial G}{\partial \eta} \text{ finite}, \quad \eta \to 0 \ (i = 1) \end{aligned} \tag{19b}$$

$$\frac{\partial G}{\partial \eta} + H_o G = 0 \quad , \quad \eta = 1 \tag{19c}$$

$$G = 0 \quad , \quad \xi < \xi_o \tag{19d}$$

The Green's function, $G(\eta,\xi\,|\eta_o,\xi_o)$ is the response function to a concentrated heat source located at (η_o,ξ_o). The arguments of the Green's function are written to emphasize their effect/cause relationship.

An important feature of this choice of the Green's function is the fact that a constant external convection coefficient is taken for the boundary condition (19c). Thus, the solution to Eqs. (19) can readily be obtained by the finite integral transform technique as outlined in Appendix B.

The delta function in the radial variable, $\delta^i(\eta - \eta_o)$, has the normal interpretation for i = 0 (parallel plates), but must be interpreted as a cylindrical delta function for i = 1 (circular tube). That

is,

$$\int_{\eta_o=o}^{1} \eta_o^i \, \delta^i(\eta - \eta_o) d\eta_o = 1 \qquad , \quad 0 \leq \eta \leq 1$$

and

$$\int_{\eta_o=o}^{1} \eta_o^i \, \phi(\eta_o)\delta^i(\eta - \eta_o) \, d\eta_o = \phi(\eta) \qquad , \quad 0 \leq \eta \leq 1$$

Proceeding formally, the governing equations (17) and (19) are rewritten in terms of the cause variables, (η_o,ξ_o), making use of the reciprocity relation for parabolic systems defined as follows,

$$G(\eta,\xi\,|\,\eta_o,\xi_o) = G(\eta_o,-\xi_o\,|\,\eta,-\xi)$$

which follows directly from the Green's function constructed in Appendix B. Equation (19a) (in cause variables) is multiplied by $\theta(\eta_o,\xi_o)$ and subtracted from equation (17a) (in cause variables) multiplied by $G(\eta,\xi\,|\,\eta_o,\xi_o)$. The result is then integrated from $\xi_o = 0$ to $\xi_o = \xi + \sigma$ and from $\eta_o = 0$ to $\eta_o = 1$, where $\sigma > 0$ is a small positive quantity. The result is

$$\int_{\xi_o=0}^{\xi+\sigma} \int_{\eta_o=0}^{1} \eta_o^i \frac{v(\eta_o)}{2} \frac{\partial}{\partial \xi_o} (G\theta) d\eta_o d\xi_o = \int_{\xi_o=0}^{\xi+\sigma} \int_{\eta_o=0}^{1} \frac{\partial}{\partial \eta_o} \left[\eta_o^i g(\eta_o)\left(G \frac{\partial \theta}{\partial \eta_o}\right.\right.$$

$$\left.\left. - \theta \frac{\partial G}{\partial \eta_o} \right)\right] d\eta_o d\xi_o + \int_{\xi_o=0}^{\xi+\sigma} \int_{\eta_o=0}^{1} \eta_o^i \, G \, S(\eta_o,\xi_o) d\eta_o d\xi_o \qquad (20)$$

$$- \int_{\xi_o=0}^{\xi+\sigma} \int_{\eta_o=0}^{1} \eta_o^i \, \theta(\eta_o,\xi_o) \, \delta^i(\eta - \eta_o) \, \delta(\xi - \xi_o) \, d\eta_o d\xi_o$$

Performing the indicated integrations, making use of the boundary conditions (17b,c) and (19b,c) and letting $\sigma \to 0$ gives the result,

$$\theta(\eta,\xi) = \int_{\xi_o=0}^{\xi} g(1)[H_o - H(\xi_o)] \, G(\eta,\xi|1,\xi_o)\theta(1,\xi_o)d\xi_o$$

$$+ \int_{\eta_o=0}^{1} \eta_o^i \frac{v(\eta_o)}{2} G(\eta,\xi|\eta_o,0)d\eta_o \qquad (21)$$

$$+ \int_{\xi_o=0}^{\xi} \int_{\eta_o=0}^{1} \eta_o^i \, S(\eta_o,\xi_o)G(\eta,\xi|\eta_o,\xi_o)d\eta_o d\xi_o$$

The first integral in equation (21) represents the effect of the variable boundary condition parameter, the second integral represents the effect of the inlet condition and the third integral arises from the source term.

Since $\theta(1,\xi_o)$ in the first integral is still unknown, equation (21) is evaluated at $\eta = 1$ and expressed in the form

$$\theta_w(\xi) = \int_{\xi_o=0}^{\xi} K(\xi,\xi_o)\theta_w(\xi_o)d\xi_o + f(\xi) \qquad (22)$$

where

$$\theta_w(\xi) = \theta(1,\xi) \qquad (23a)$$

$$K(\xi,\xi_o) = g(1)[H_o - H(\xi_o)]\, G(1,\xi\,|\,1,\xi_o) \tag{23b}$$

$$f(\xi) = \int_{\eta_o=0}^{1} \eta_o^i \frac{v(\eta_o)}{2}\, G(1,\xi\,|\,\eta_o,0)\,d\eta_o + \int_{\xi_o=0}^{\xi}\int_{\eta_o=0}^{1} \eta_o^i\, S(\eta_o,\xi_o)\, G(1,\xi\,|\,\eta_o,\xi_o)\, d\eta_o d\xi_o \tag{23c}$$

have been defined for convenience.

Equation (22) is a singular Volterra integral equation of the second kind for the wall temperature, which could be resolved if a suitable numerical integration procedure was available. However, there is a numerical difficulty inherent in equation (22) which makes direct numerical integration impossible. This difficulty is the singularity of the kernel, $K(\xi,\xi_o)$, when its arguments are equal. The singularity arises from the Green's function at the point where the concentrated heat source is located. Since the Green's function is the response function to the concentrated heat source, it becomes unbounded at that point.

To overcome this difficulty, the following singularity subtraction procedure is used to rewrite equation (22) as

$$\theta_w(\xi) = \int_{\xi_o=0}^{\xi-\Delta\xi} K(\xi,\xi_o)\theta_w(\xi_o)d\xi_o + \int_{\xi_o=\xi-\Delta\xi}^{\xi} K(\xi,\xi_o)[\theta_w(\xi_o) - \theta_w(\xi)]d\xi_o + \theta_w(\xi)\int_{\xi_o=\xi-\Delta\xi}^{\xi} K(\xi,\xi_o)d\xi_o + f(\xi) \tag{24}$$

where $\Delta\xi$ is the step size used in the numerical integration. Equation (24) is now in a form suitable for direct numerical integration. The integrand in the first integral contains all bounded values, hence it provides no difficulties. The integrand in the second integral vanishes at the upper limit of integration, successfully cancelling the singular point of the kernel. The third integral in equation (24) contains only the kernel, which although singular, is integrable with analytical expressions available for many variations of the heat transfer coefficient.

In order to numerically integrate equation (24), it is necessary to choose an integration scheme. The trapezoid rule is chosen due to its combination of simplicity and accuracy. Discretization of Eq. (24) and rearranging gives,

$$\theta_w(\xi_N) = \frac{f(\xi_N) + \frac{\Delta\xi}{2} K(\xi_N,0) + \sum_{j=2}^{N-2} \Delta\xi K(\xi_N,\xi_j)\theta_w(\xi_j) + \int_{\xi_o=\xi_{N-1}}^{\xi_N} K(\xi_N,\xi_o)d\xi_o}{1 + \frac{\Delta\xi}{2} K(\xi_N,\xi_{N-1})} \quad , N = 2,3,... \tag{25}$$

where $\xi_j = (j - 1)\Delta\xi$ and $\theta_w(\xi_1) = 1$ have been used. The integral containing the kernel in Eq. (25) has not been numerically integrated to allow for an analytical expression. Equation (25) is a recurrence relation for the wall temperature which is directly suitable for digital computation.

Another quantity of interest is the bulk temperature, defined as

$$\theta_b(\xi) = 2^i \int_{\eta=0}^{1} \eta^i v(\eta)\theta(\eta,\xi)\, d\eta \tag{26}$$

An expression for $\theta_b(\xi)$ can be obtained by multiplying the thermal energy equation, (17a) with $2^{i+1}\eta^i$ and integrating from $\eta = 0$ to $\eta = 1$.

The result can be written as follows

$$\theta_b(\xi) = 1 - 2^{i+1} \int_{\xi'=0}^{\xi} g(1)H(\xi')\theta_w(\xi')d\xi' \tag{27}$$

$$+ 2^{i+1} \int_{\xi'=0}^{\xi} \int_{\eta=0}^{1} \eta^i S(\eta,\xi')d\eta d\xi'$$

Since values for the wall temperature are already available, the bulk temperature is immediately obtained from a numerical integration of Eq. (27). In the absence of energy sources, (S = 0), the trapezoid rule gives,

$$\theta_b(\xi_N) = \theta_b(\xi_{N-1}) - 2^{i+1}g(1)\frac{\Delta\xi}{2}\left[H(\xi_{N-1})\theta_w(\xi_{N-1})\right. \tag{28}$$

$$\left. + H(\xi_N)\theta_w(\xi_N)\right]$$

A quantity of great engineering interest is the dimensionless, total heat transfer, $Q(\xi)$, defined as the ratio of the heat transferred from the fluid at some axial location ξ to the total heat transferred from the fluid as a condition of thermal saturation is reached. In the absence of energy sources,

$$Q(\xi) = 1 - \theta_b(\xi) \tag{29}$$

The Nusselt number, or internal heat transfer coefficient can be expressed as,

$$Nu = \frac{2H(\xi)\theta_w(\xi)}{\theta_b(\xi) - \theta_w(\xi)} \tag{30}$$

The solution is now complete with the wall and bulk temperatures available from Eqs. (25) and (28), respectively. The Green's function necessary to form the kernel of the finite integral equation is derived in Appendix B using the integral transform technique. The solutions to the corresponding eigenvalue problems for each of the possible flow types are presented in Appendix A.

V. RESULTS AND DISCUSSION

The most basic elements required in the solution methodology are the velocity profile and related eddy diffusivity as given by Eqs. (16) and (15g), respectively. These two functions appear in every aspect of the problem including the eigenvalue problem, the Green's function equations and the integral equation. Therefore, an understanding of these two functions is crucial to an understanding of the results which follow. Figure 3a shows the dimensionless total diffusivity as given by Eq. (15g) for slug, laminar and turbulent flow in a pipe. The total diffusivity represents the sum of molecular and turbulent diffusion of heat in the radial direction. In slug and laminar flow the total diffusivity, $g(\eta) = 1$, due to the absence of turbulent mixing in these cases. In turbulent flow, the total diffusivity varies from $g(\eta) = 1$ at the wall to a maximum near $\eta = 0.6$ and then drops slightly near the center of the pipe. As Re increases, the total diffusivity increases due to an increase in the mixing intensity, yet even at the relatively low Re = 5,000 the turbulent diffusivity dominates the molecular diffusivity except in the near wall region.

In Figure 3b, the velocity profiles for slug, laminar and turbulent flow in a pipe are presented for identical mass flow rates. The slug flow profile is the result of an invsicid fluid, hence it need not satisfy the no-slip condition at the boundary. Although this is not a physically realizable situation, it provides a good approximation to some real situations. The laminar profile is seen to have a low velocity in the wall region with a relatively high velocity near the pipe center. The time-averaged turbulent velocity profiles, obtained by

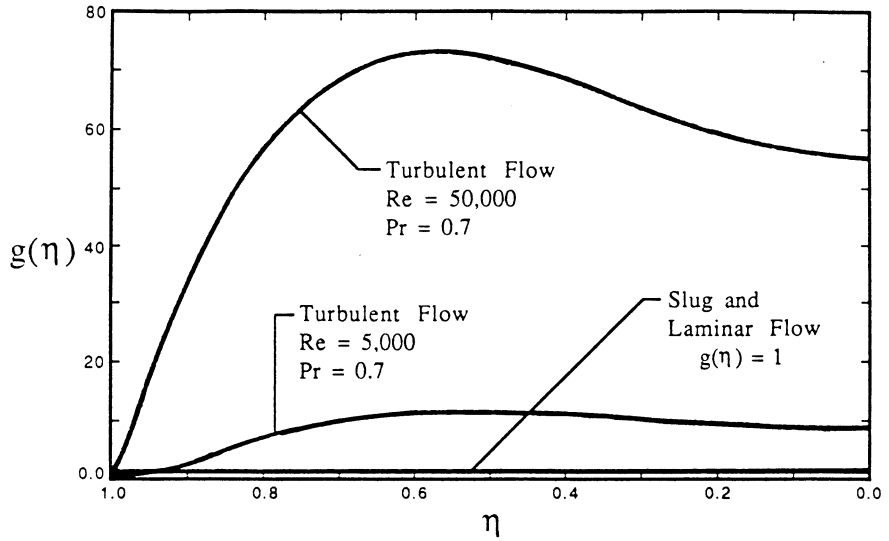

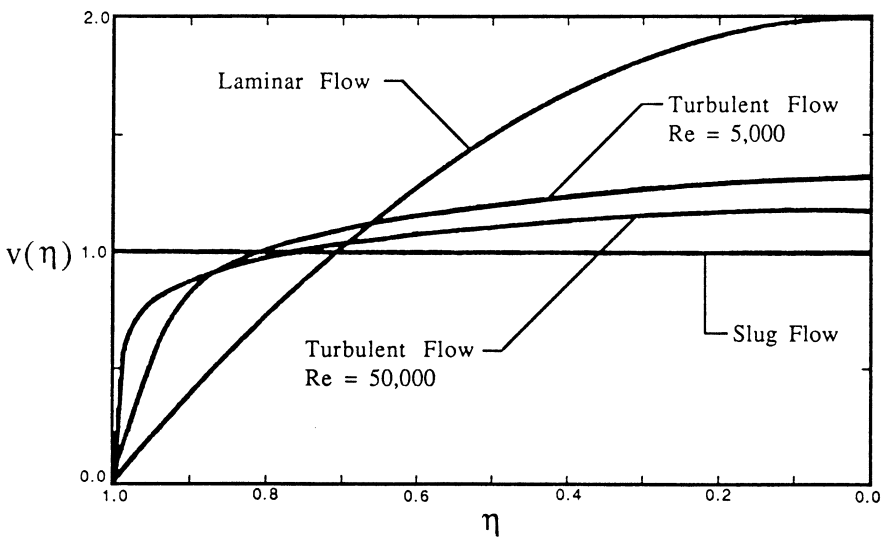

Figure 3. (a) Dimensionless total diffusivities
(b) Dimensionless velocity profiles

numerical integration of Eq. (16d) exhibit some similarities with both slug and laminar flow. The turbulent velocity profiles must satisfy the no-slip condition at the wall, as in laminar flow, yet have a rather flat shape away from the wall due to the turbulent mixing of momentum. In fact, as $Re \to \infty$, the time-averaged turbulent velocity profile approaches the slug flow profile.

The eddy diffusivity variations and velocity profiles for the flow models presented in Fig. 3 show up directly in the eigenvalue problem as given by the system of Eqs. (A1) in Appendix A. Each choice of geometry and flow model results in a distinct eigenvalue problem. The methods of solution of the eigenvalue problems for slug flow in a tube, laminar flow in a tube and turbulent flow in a tube are discussed in Appendix A.

Figure 4 shows the first five normalized eigenfunctions for the three cases mentioned above. Figure 4a shows the well-known Bessel functions. Figure 4b shows the Graetz functions and, Fig. 4c shows the turbulent eigenfunctions. Each set of eigenfunctions displays some similarities with the others. For example, $\psi_m(1)$ alternates in sign for consecutive m in each case. However, the Graetz and Bessel eigenfunctions can be enclosed in a uniformly decaying envelope whereas the turbulent eigenfunctions appear to peak up near $\eta = 1$. It is interesting to note how similar each of the three cases appear even though they have very different velocity and eddy diffusivity variations.

To examine the eigenvalue problem solutions further, Table 2 presents the first ten eigenvalues and normalized eigenfunctions at the wall for both slug and laminar flow in a tube, for different values of

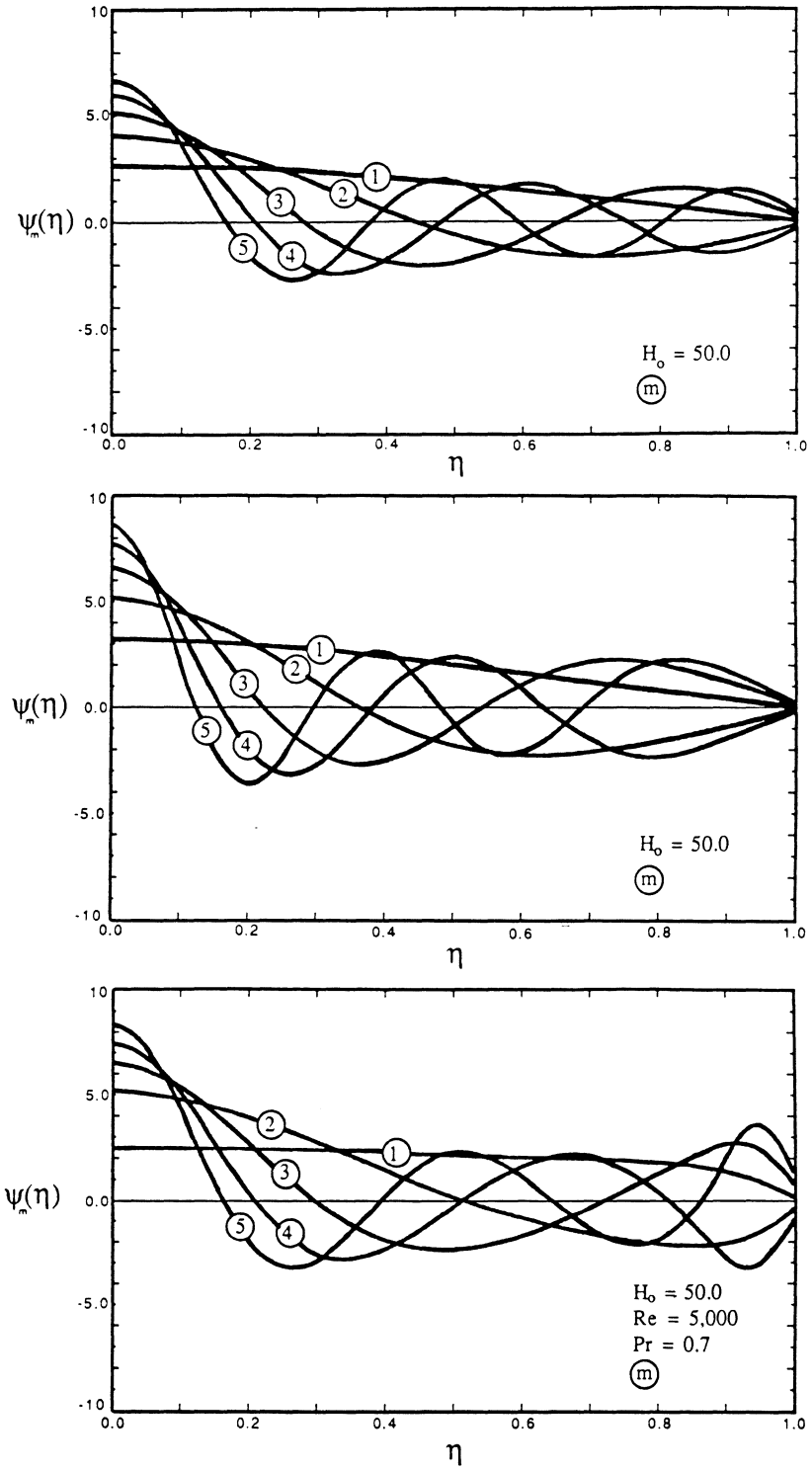

Figure 4. Normalized eigenfunctions for
(a) Slug flow, (b) Laminar flow, (c) Turbulent flow

Table 2. Eigenvalues and normalized eigenfunctions for slug and laminar pipe flow

		$H_o = 1$		$H_o = 5$		$H_o = 50$		$H_o = \infty$	
	m	λ_m	$\psi_m(1)$	λ_m	$\psi_m(1)$	λ_m	$\psi_m(1)$	λ_m	$\psi_m(1)$
Slug flow in a tube (Bessel Functions)	1	1.776	1.565	2.814	0.739	3.334	0.094	3.401	0.000
	2	5.769	-1.942	6.665	-1.372	7.653	-0.215	7.807	0.000
	3	10.120	1.981	10.773	1.672	11.998	0.335	12.238	0.000
	4	14.525	-1.991	15.022	-1.810	16.351	-0.451	16.676	0.000
	5	18.948	1.994	19.344	1.878	20.709	0.562	21.115	0.000
	6	23.379	-1.996	23.706	-1.917	25.070	-0.668	25.556	0.000
	7	27.813	1.997	28.092	1.939	29.435	0.769	29.998	0.000
	8	32.250	-1.998	32.492	-1.954	33.803	-0.863	34.440	0.000
	9	36.688	1.998	36.902	1.964	38.176	0.950	38.882	0.000
	10	41.127	-1.999	41.319	-1.971	42.551	-1.031	43.324	0.000
Laminar flow in a tube (Graetz Functions)	1	1.641	1.333	2.356	0.527	2.664	0.064	2.684	0.000
	2	5.478	-1.893	6.135	-0.978	6.608	-0.134	6.643	0.000
	3	9.436	2.133	10.013	1.281	10.578	0.196	10.624	0.000
	4	13.415	-2.290	13.931	-1.506	14.555	-0.253	14.611	0.000
	5	17.403	2.409	17.871	1.683	18.535	0.306	18.600	0.000
	6	21.394	-2.505	21.825	-1.828	22.517	-0.356	22.590	0.000
	7	25.387	2.586	25.788	1.951	26.501	0.404	26.581	0.000
	8	29.382	-2.657	29.757	-2.057	30.485	-0.450	30.573	0.000
	9	33.378	2.720	33.731	2.150	34.471	0.494	34.565	0.000
	10	37.375	-2.776	37.709	-2.233	38.458	-0.537	38.557	0.000

the boundary condition parameter, H_o. It can be seen that the eigenvalues of the Bessel functions increase asymptotically by 4.4 while the eigenvalues of the Graetz functions increase by 4.0 asymptotically as $m \to \infty$. The normalized eigenfunctions at the wall alternate in sign for both cases as m increases. In the case of slug flow, the normalized Bessel functions at $\eta = 1$ tend to a limit in absolute value, but the normalized Graetz functions increase without bound in absolute value as $m \to \infty$. The boundary condition parameter, H_o, has only a slight effect on the eigenvalues in both cases. As H_o increases each eigenvalue experiences a slight positive shift which decays for large eigenvalues. H_o has a profound effect on the normalized eigenfunctions, however. As H_o increases, the normalized eigenfunctions become increasingly smaller with the case $H_o = \infty$ corresponding to the constant wall temperature situation.

The eigenvalues and normalized eigenfunctions for the case of turbulent flow in a tube are presented in Table 3 for sixteen different combinations of the parameters Re, Pr and H_o. Many of the trends seen in Table 2 are evident here as well. An increase in H_o has much the same effect for all choices of Re and Pr as in laminar or slug flow. For turbulent flow, the asymptotic difference between consecutive eigenvalues is much larger than in slug or laminar flow. As Re or Pr increase, the eigenvalues appear to grow much more quickly. The normalized eigenfunctions are affected slightly by an increase in Re, as seen in Table 3.

The eigenvalues and normalized eigenfunctions show up directly in the Green's function as shown in Appendix B. Clearly, the Green's

Table 3. Eigenvalues and normalized eigenfunctions for turbulent pipe flow

		$H_o = 1$		$H_o = 5$		$H_o = 50$		$H_o = \infty$	
	m	λ_m	$\psi_m(1)$	λ_m	$\psi_m(1)$	λ_m	$\psi_m(1)$	λ_m	$\psi_m(1)$
Re = 5,000 Pr = 0.7	1	1.898	1.801	3.580	1.277	5.445	0.291	5.879	0.000
	2	16.886	-2.541	17.452	-1.907	18.586	-0.470	18.932	0.000
	3	28.279	3.629	29.005	2.851	30.644	0.741	31.166	0.000
	4	39.278	-4.228	40.038	-3.545	42.150	-1.042	42.911	0.000
	5	50.511	4.349	51.168	3.822	53.414	1.297	54.381	0.000
Re = 50,000 Pr = 0.7	1	1.991	1.973	4.301	1.841	10.236	1.039	14.646	0.000
	2	43.651	-2.414	43.903	-2.282	45.514	-1.398	47.869	0.000
	3	75.252	3.125	75.498	2.967	77.136	1.866	79.724	0.000
	4	106.361	-3.734	106.611	-3.559	108.327	-2.294	111.210	0.000
	5	137.227	4.299	137.484	4.111	139.302	2.706	142.511	0.000
Re = 5,000 Pr = 5.0	1	1.950	1.900	3.977	1.580	7.380	0.543	8.637	0.000
	2	42.287	-3.356	42.727	-2.785	44.082	-0.934	44.740	0.000
	3	67.781	6.315	68.776	5.357	71.979	1.828	73.481	0.000
	4	91.015	-7.515	92.129	-6.755	96.708	-2.736	99.329	0.000
	5	116.704	7.553	117.584	6.892	121.910	3.208	124.979	0.000
Re = 50,000 Pr = 5.0	1	2.003	1.997	4.424	1.947	12.368	1.521	25.045	0.000
	2	115.723	-2.487	115.828	-2.429	116.734	-1.928	120.132	0.000
	3	199.300	3.349	199.410	3.272	200.368	2.601	204.010	0.000
	4	281.312	-4.228	281.436	-4.131	282.520	-3.285	286.637	0.000
	5	362.345	5.217	362.491	5.097	363.773	4.049	368.584	0.000

function is of central importance in the solution of the integral equation (22). One dominant characteristic of the Green's function as given by equation (B7) in Appendix B is its singularity as $\xi_o \to \xi$. For slug and laminar flow, the Green's function is presented as a function of $\Delta\xi = \xi - \xi_o$ in Fig. 5. Clearly, as $\Delta\xi \to 0$, the Green's function grows increasingly larger. The laminar flow case yields a Green's function that is larger than the Green's function for slug flow because the eigenfunctions are larger in absolute value in laminar flow while the eigenvalues do not grow as quickly. The Green's functions decrease quite a bit for a moderate increase in H_o because of slightly increased eigenvalues and decreased values of the normalized eigenfunctions evaluated at the wall.

In turbulent flow, the Green's function must be presented as a function of $\frac{\Delta z}{r_o} = \Delta\xi RePr$ to make sense of the dependence of the Green's function on the parameters Re and Pr. Figure 6 shows the dependence of the Green's function on Re. Apparently, the Green's function becomes more singular as Re grows large, however, an inspection of the eigenvalues in Table 3 would lead to the opposite conclusion. In the tube coordinates, $\frac{\Delta z}{r_o}$, however, the $\Delta\xi$ axis is effectively compressed to yield the results as shown. Figure 7 shows a similar effect of Pr on the Green's function. Note that an order of magnitude increase in Pr has a rather drastic effect on the Green's function. The results shown in Fig. 8 have the same trend as in the laminar and slug flow case with the Green's function becoming smaller as $H_o \to \infty$.

Another critical aspect of the Green's function in which the eigenvalues play a dominant role is the convergence of the infinite sum of

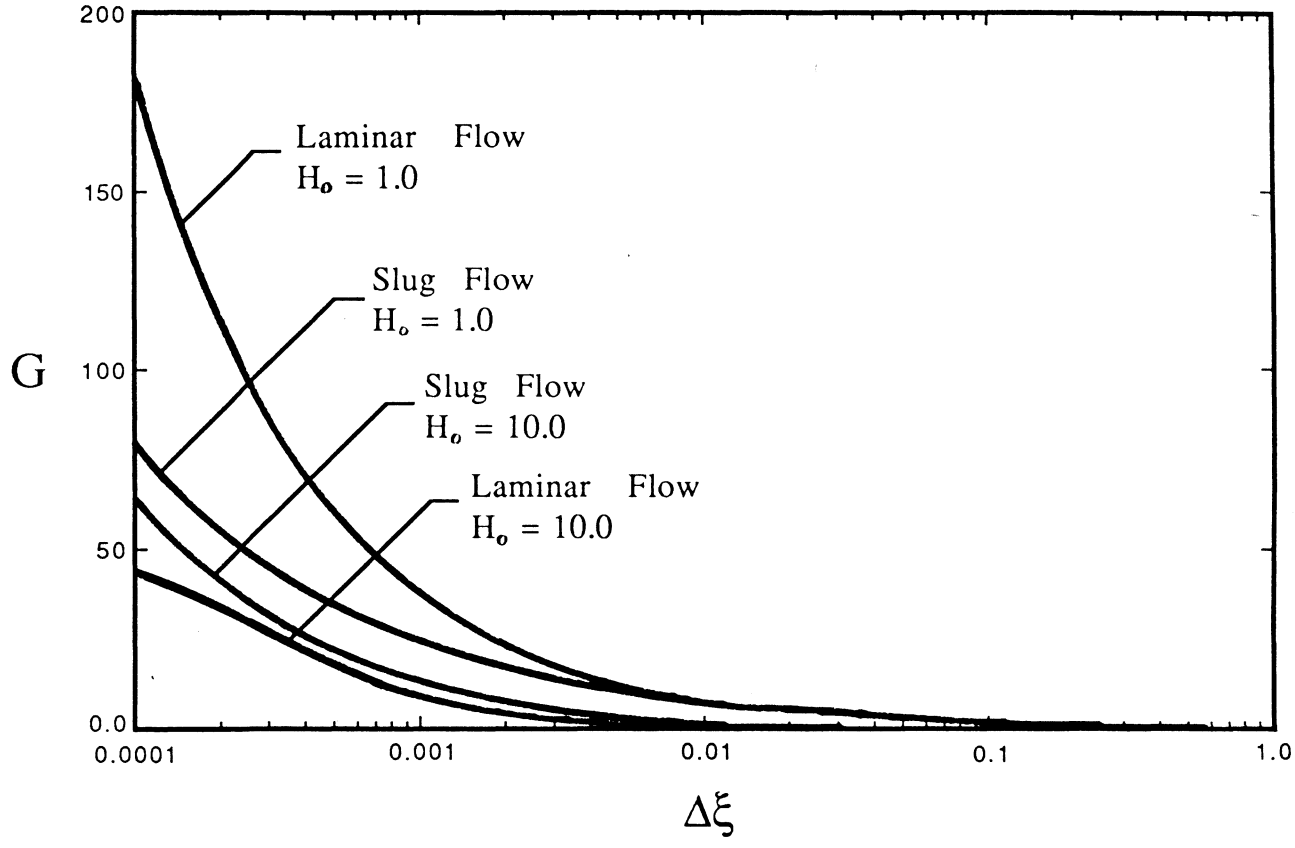

Figure 5. Green's functions for slug and laminar flow showing the effect of H_o.

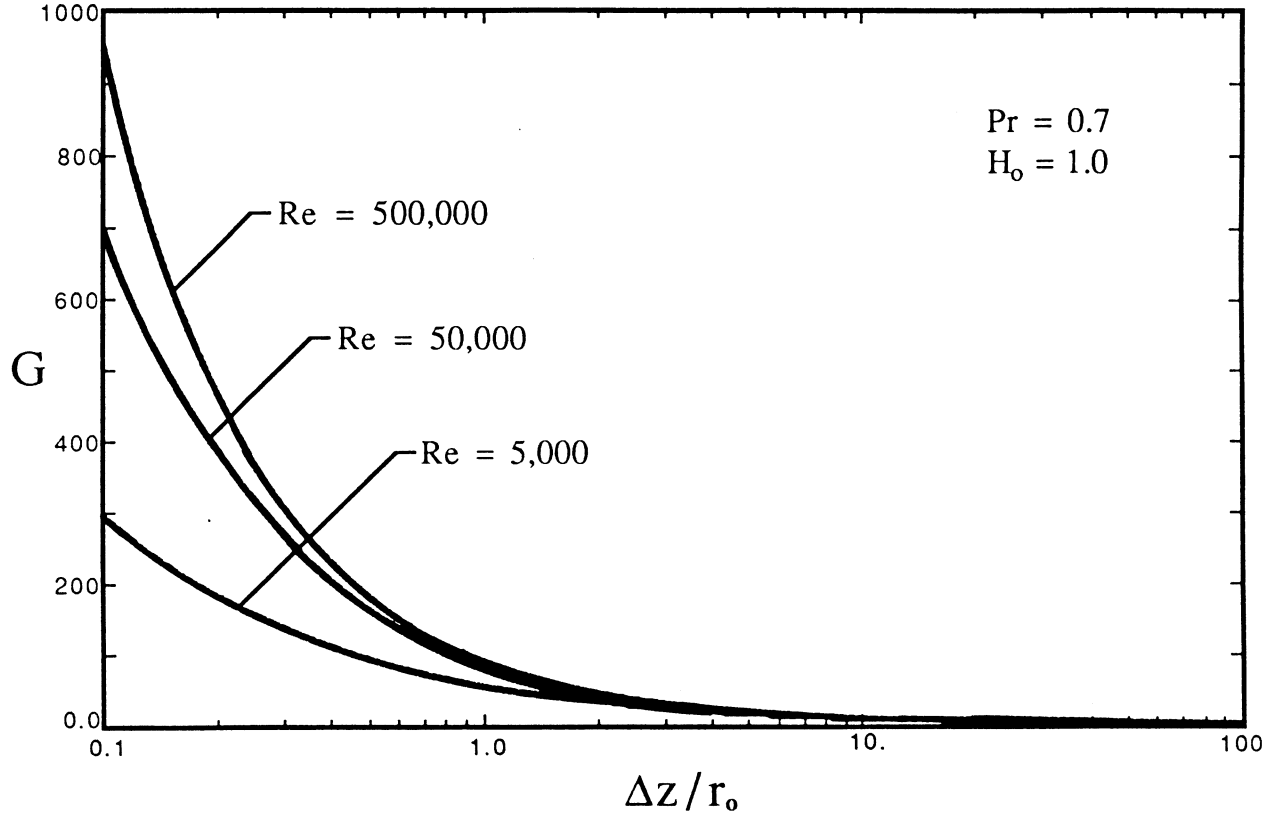

Figure 6. Green's functions for turbulent flow showing the effect of Re

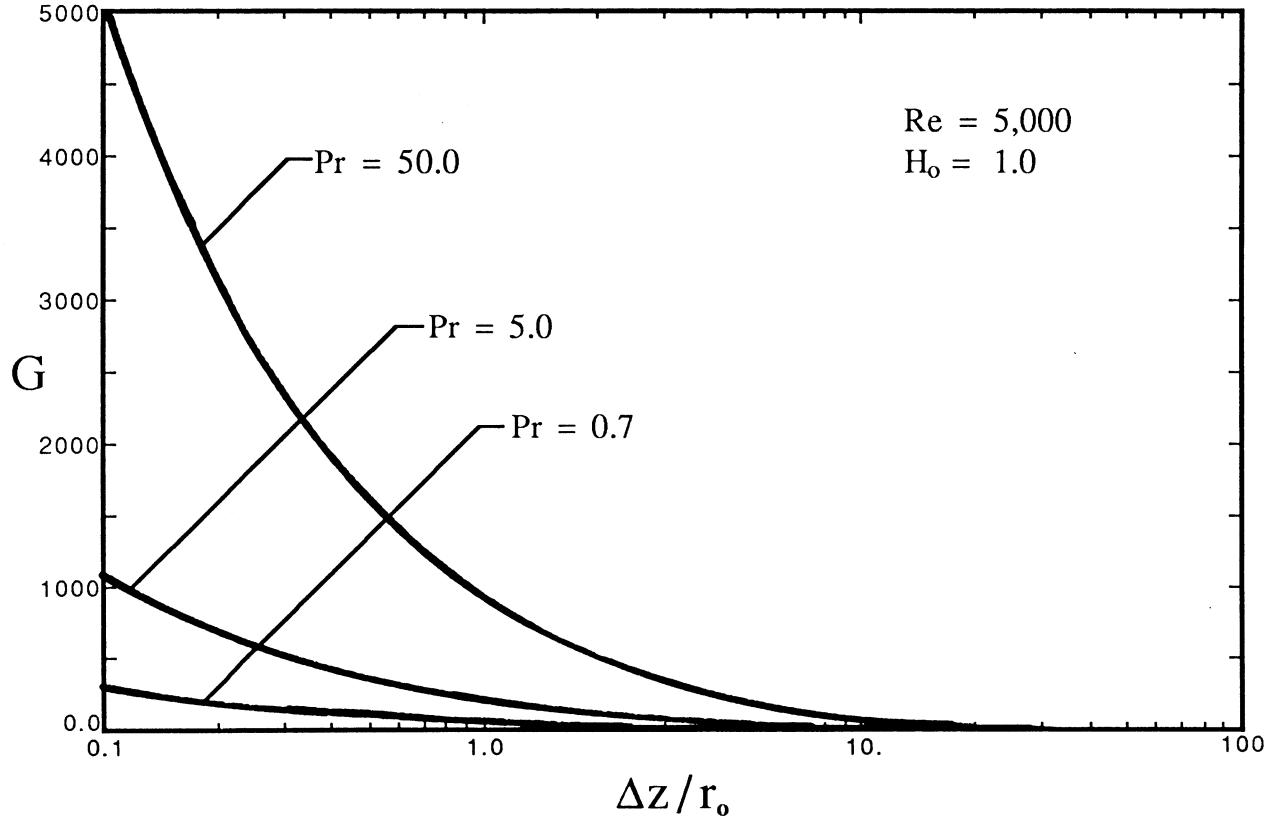

Figure 7. Green's functions for turbulent flow showing the effect of Pr

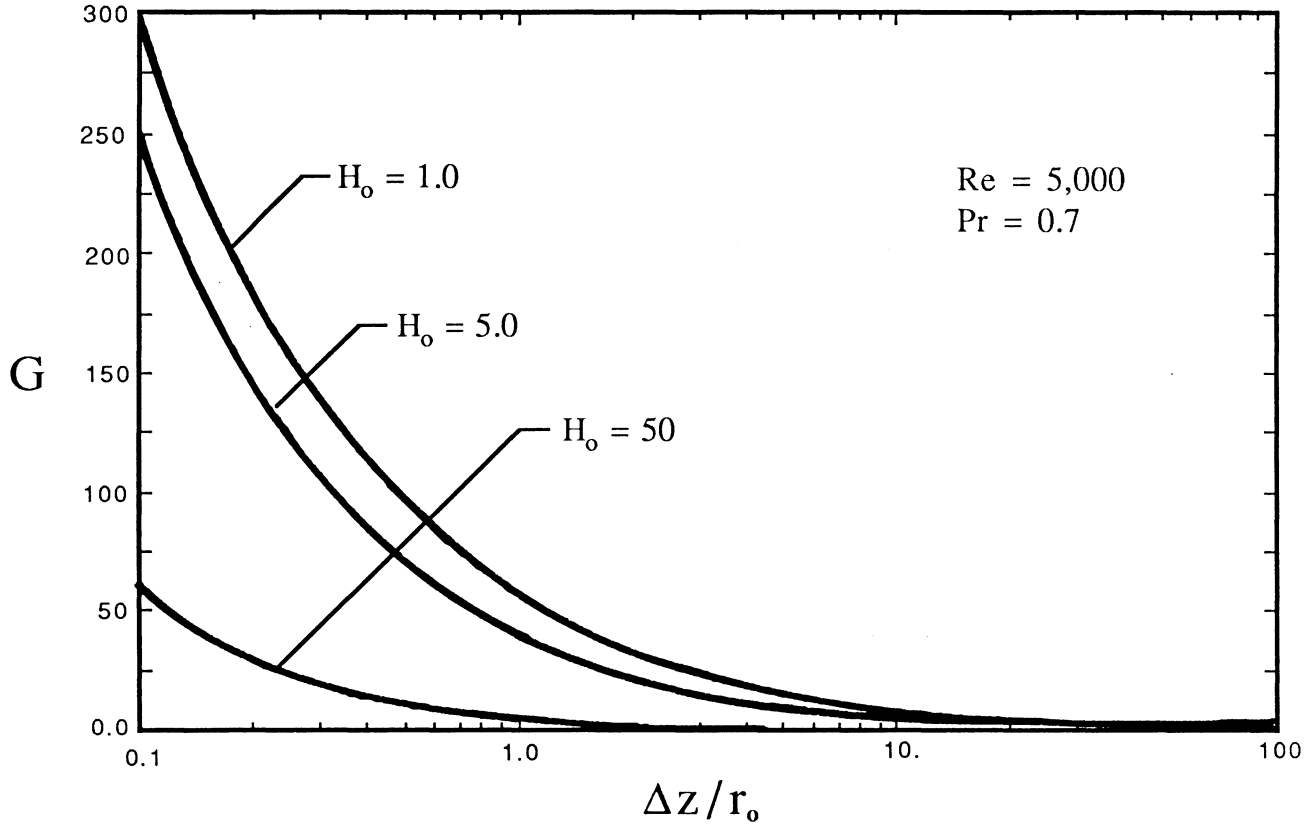

Figure 8. Green's function for turbulent flow showing the effect of H_o

Eq. (B7). The main reason to analyze the convergence of the Green's function is to determine how many eigenvalues must be calculated. It is important to make sure that sufficient eigenvalues have been obtained to ensure convergence of the infinite sum, without using too many, since the calculation of the eigenvalues is one of the most computationally demanding aspects of the solution procedure, especially for turbulent flow. Table 4 shows how many terms in the infinite series are required to obtain convergence of expression (B7) to within 99.9% of its final value. In a typical solution for laminar flow with $\xi_1 = 0.003$ and $\xi_2 = 0.001$, the axial step size, $\Delta\xi = \xi - \xi_o$, would probably be chosen as $\Delta\xi = 0.0001$ which means that a maximum of 68 eigenvalues would be required. The Green's function does not converge as rapidly for the laminar flow case since the Graetz eigenvalues do not grow as quickly as the Bessel eigenvalues.

The results of the convergence analysis for turbulent flow are presented in Table 5. These results are presented in terms of $\frac{\Delta z}{r_o}$ in order to make a valid comparison between cases with different Re and Pr moduli. An examination of the eigenvalues presented in Table 3 would lead to the conclusion that for higher Re and Pr the convergence rate of the Green's function would be significantly better, however this is not the case. The reason for this lies in the fact that for a constant value of $\frac{\Delta z}{r_o}$, the higher the values chosen for Re and Pr, the smaller the resulting value of $\Delta\xi = \frac{\Delta z}{(r_o RePr)}$. Thus, the effect of larger eigenvalues and smaller $\Delta\xi$ essentially offset each other, with the result that the number of terms needed in the infinite series remains fairly constant as Re and Pr are varied.

Table 4. Number of terms required for convergence of the Green's function to 99.9% of its final value in slug and laminar pipe flow

	$H_o = 1$			$H_o = 50$		
Case \ $\Delta\xi$	10^{-5}	10^{-4}	10^{-3}	10^{-5}	10^{-4}	10^{-3}
Slug Flow	166	53	17	171	57	20
Laminar Flow	194	62	20	208	68	22

Table 5. Number of terms required for convergence of the Green's function to 99.9% of its final value in turbulent pipe flow

	$H_o = 1$			$H_o = 50$		
$\Delta z / r_o$ / Case	0.05	0.10	1.0	0.05	0.10	1.0
Re = 5,000 Pr = 0.7	56	40	13	60	43	14
Re = 50,000 Pr = 0.7	67	48	16	69	50	17
Re = 5,000 Pr = 5.0	66	47	15	69	48	15

With the Green's function available from Eq. (B7) in Appendix B, the solution of the integral equation (22) can now be accomplished. The integration of Equation (24) by the trapezoid rule is presented in the Analysis section with the discretized form of the integral equation given by Eq. (25). In the solution of Eq. (25), the exponentially decaying nature of the Green's function can be used to good advantage by reducing the number of terms required in the summation term in the numerator as $\Delta\xi$ becomes large. Since the Green's function decays very rapidly for large $\Delta\xi$, the wall temperatures far upstream from the current axial location cease to play a significant role and can be neglected. This results in considerable savings in computer time and storage.

The trapezoid rule is chosen for the numerical integration of Eq. (24) because it produces results indistinguishable from those using a finite difference scheme for laminar flow [2]. There do not appear to be any results in the literature dealing with a turbulent flow and a variable Biot number for comparison. For this reason, and to ensure that the numerical scheme produces valid results, numerical experiments were conducted demonstrating that the solution of the integral equation becomes independent of the mesh size chosen as $\Delta\xi \to 0$. An analysis of the convergence, round-off error and stability for a general quadrature method is presented in reference [64]. If higher accuracy is desired than the trapezoid rule, a block method can be employed [64]. Overall, the most important numerical parameter is the step size, $\Delta\xi$, since it affects both the accuracy of the numerical integration of Eq. (24) and the convergence of the Green's function given by Eq. (B7).

The analysis is carried out in terms of ξ for slug, laminar and turbulent flow. The results which follow for slug and laminar flow are presented in terms of ξ since the effect of Re and Pr can be totally absorbed in the axial variable ξ. In turbulent flow, the results must be presented in terms of $\frac{z}{r_o}$ since both the dimensionless velocity profile and the eddy diffusivity depend directly on Re and Pr. Presenting the results in terms of $\frac{\Delta z}{r_o}$ allows a meaningful parameter study of Re and Pr to be presented. Also, all results are presented for the tube geometry since this geometry is considerably more important for practical applications than the parallel plates.

Figure 9 shows the wall and bulk temperatures for laminar flow in a tube for both stepwise periodic and harmonic variations of the Biot number. The wall temperature for the stepwise periodic case drops sharply in regions of high H and then rises sharply in regions of low H. In this case, the value $H_1 = 1$ is low enough so as to cause an insulating effect in the unfinned region. For the harmonic case, the wall temperature rises and falls more gradually, as would be expected from a gradually changing convection coefficient. Although the wall temperature settles into a repetitive pattern, the magnitude is steadily dropping in each successive cycle as the fluid approaches the dimensionless ambient temperature of zero.

Consistent with basic energy considerations, the bulk temperatures shown in Fig. 9 continually decline. The stepwise periodic case shows a small drop in regions of low H and a larger drop in regions of high H. The most severe drops occur at the beginning of a high Biot number region, since the wall temperature has just risen to its greatest value

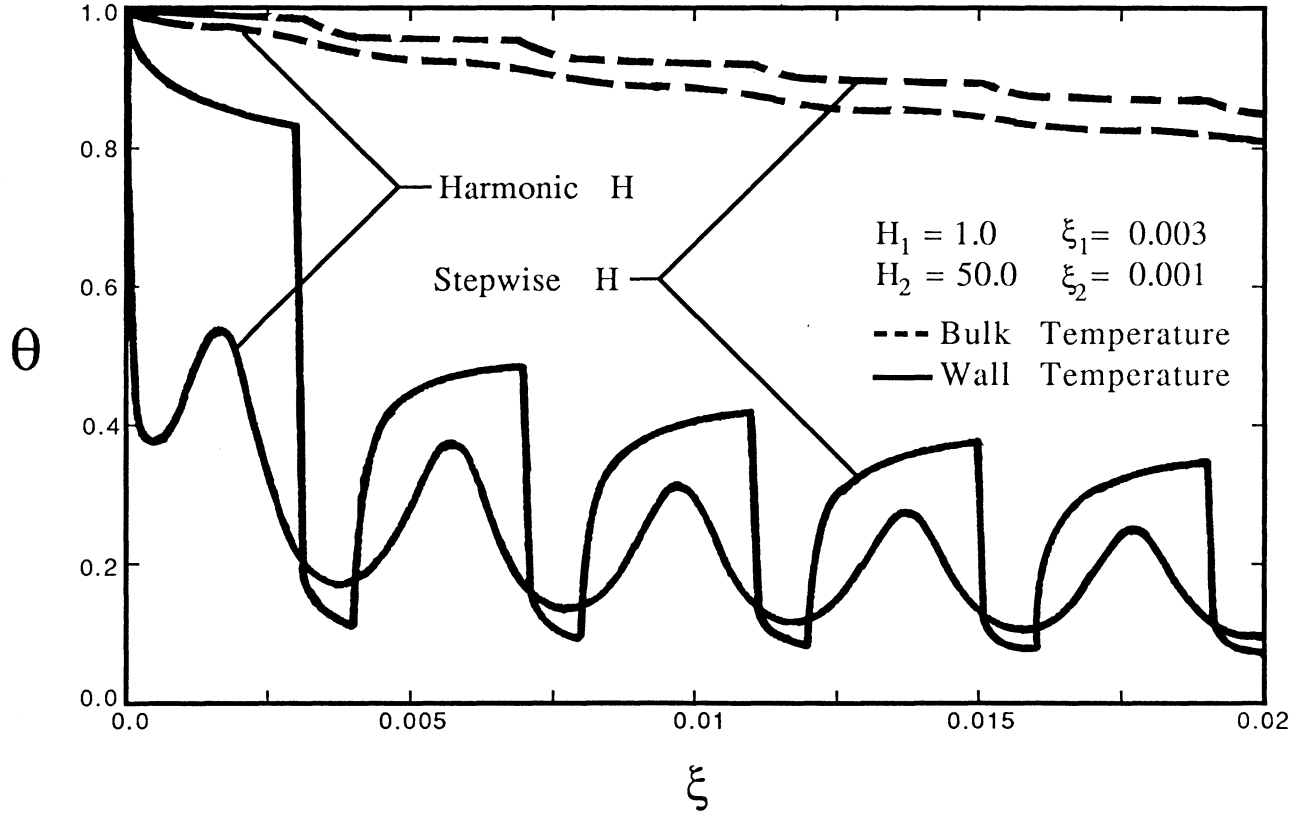

Figure 9. Wall and bulk temperatures for stepwise and harmonic variations of the external convection coefficient and laminar pipe flow

during the cycle. The bulk temperature curve for the harmonic case drops in a more steady fashion in response to the more gradual changes in Biot number. Although the average Biot number is identical for both cases, the bulk temperature is lower in the harmonic case, indicating a greater amount of heat removed from the fluid. As a result, the effect of the smoothing of the heat transfer coefficient by axial conduction in the tube wall is expected to be advantageous for heat exchanger applications where external fins are required.

Figure 10 shows results similar to those of Fig. 9 except the value of H_2 has been lowered to 5. The wall temperatures have the same characteristics as in Fig. 9, except that the magnitudes are higher due to a decrease in heat transfer. In this case, however, the bulk temperatures for the two variations are nearly identical, with the harmonic distribution still slightly lower. Thus the precise distribution of the heat transfer coefficient is more important in calculating heat transfer when a relatively large degree of enhancement (large H_2) or very effective fins are used.

Figure 11 shows the wall and bulk temperatures for slug flow in a tube for both stepwise and harmonic variations of the heat transfer coefficient. The convection coefficient variations are identical with the ones used in Fig. 10. The wall temperatures for the slug flow react much less to a change in convection coefficient than the wall temperatures for laminar flow. This is due to the fact that the velocity of the fluid at the wall is zero for laminar flow, while in slug flow the fluid at the wall is moving too fast to permit much of a temperature change. Another interesting point is that the bulk temperature drops

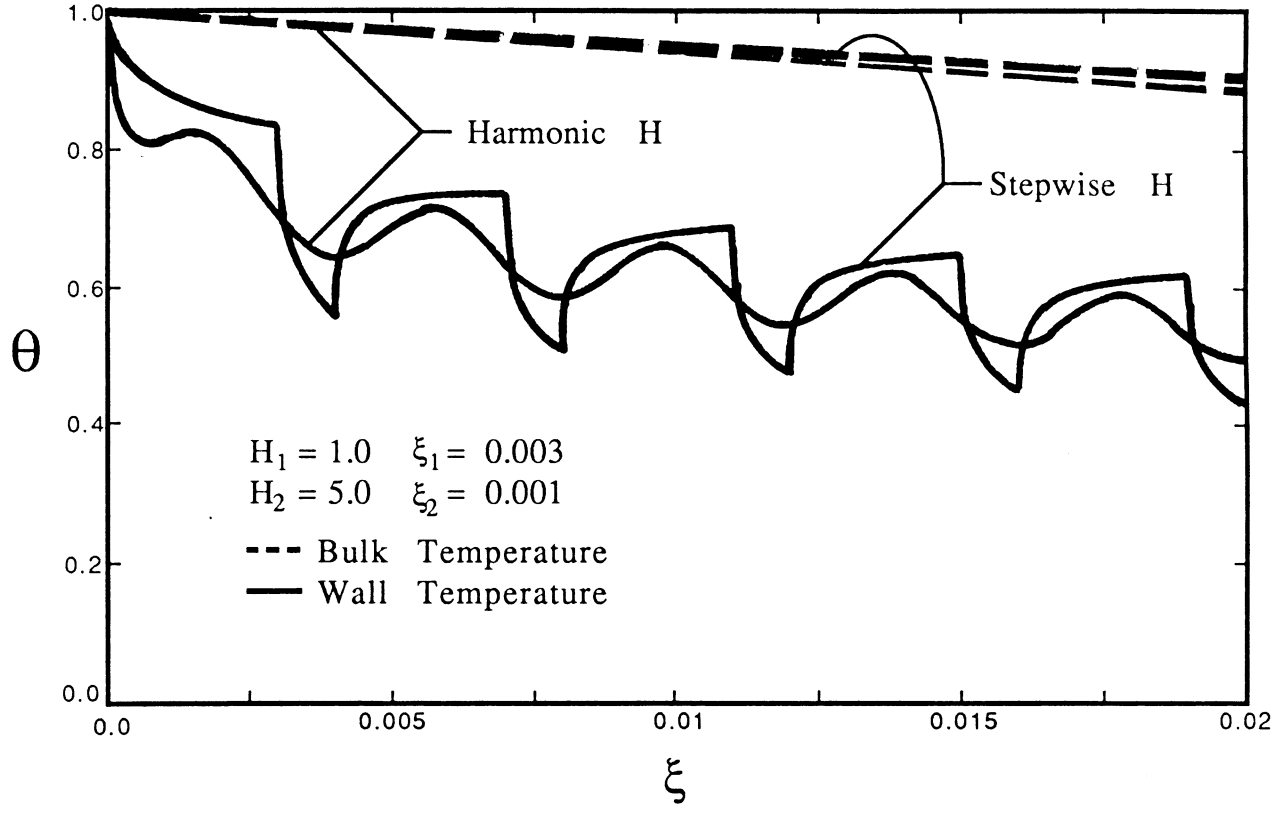

Figure 10. Wall and bulk temperatures for stepwise and harmonic variations of the external convection coefficient and laminar pipe flow

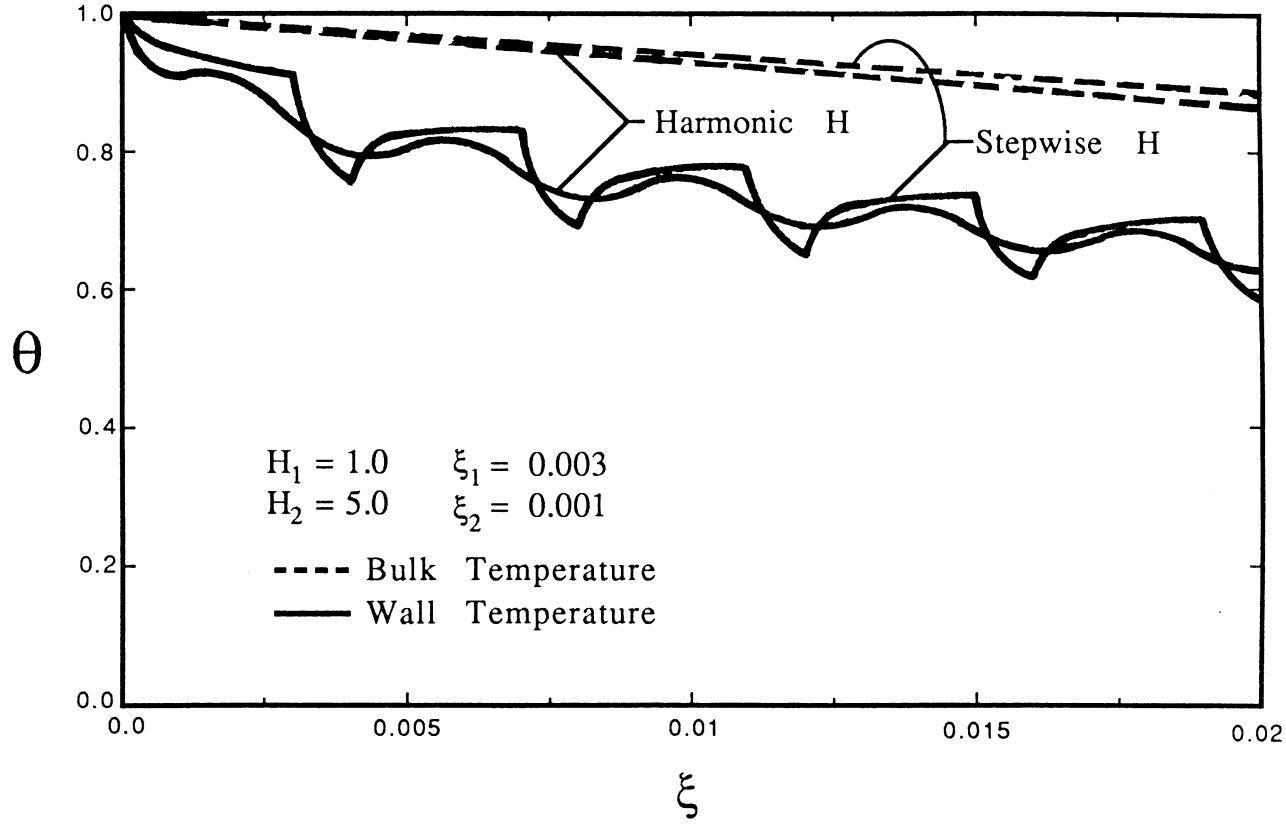

Figure 11. Wall and bulk temperatures for stepwise and harmonic variations of the external convection coefficient and slug flow in a pipe

more quickly in slug flow than in laminar flow. Again, this is due to the nonzero velocity at the wall for slug flow which effectively reduces the internal resistance to heat flow.

Figure 12 shows the wall temperatures for fully developed turbulent flow in a pipe as a function of Re for stepwise periodic H. The bulk temperatures are not shown simply because they are nearly indistinguishable from one for the first few cycles shown. As in the laminar and slug flow plots, the wall temperature drops rapidly in regions of high H and climbs in regions of low H due to the insulating effect. The effect is more pronounced at the lower Re since the lower velocity in the wall region allows more time for the heat transfer to affect the wall temperature. It is quite interesting that at the lower Re the wall temperature variations resemble those of laminar flow. This is due to the low velocity near the wall in turbulent flow and the small eddy diffusivity. As Re increases, and the turbulent velocity profile tends toward the slug flow profile, the wall temperature results appear more similar to those of slug flow. However, the increased mixing in the higher Re case (manifested through an increased eddy diffusivity) causes the wall temperature to climb more rapidly in regions of low H and to drop less severely in regions of high H.

In Fig. 13, the effect of Pr on the wall temperature for a stepwise periodic variation of the Biot number is explored. Figure 13 can be understood by examining the dimensionless eddy diffusivity obtained when the governing energy equation (17a) is rewritten in terms of $\frac{z}{r_o}$. After dividing expression (15g) by Re Pr, the total diffusivity is expressed as

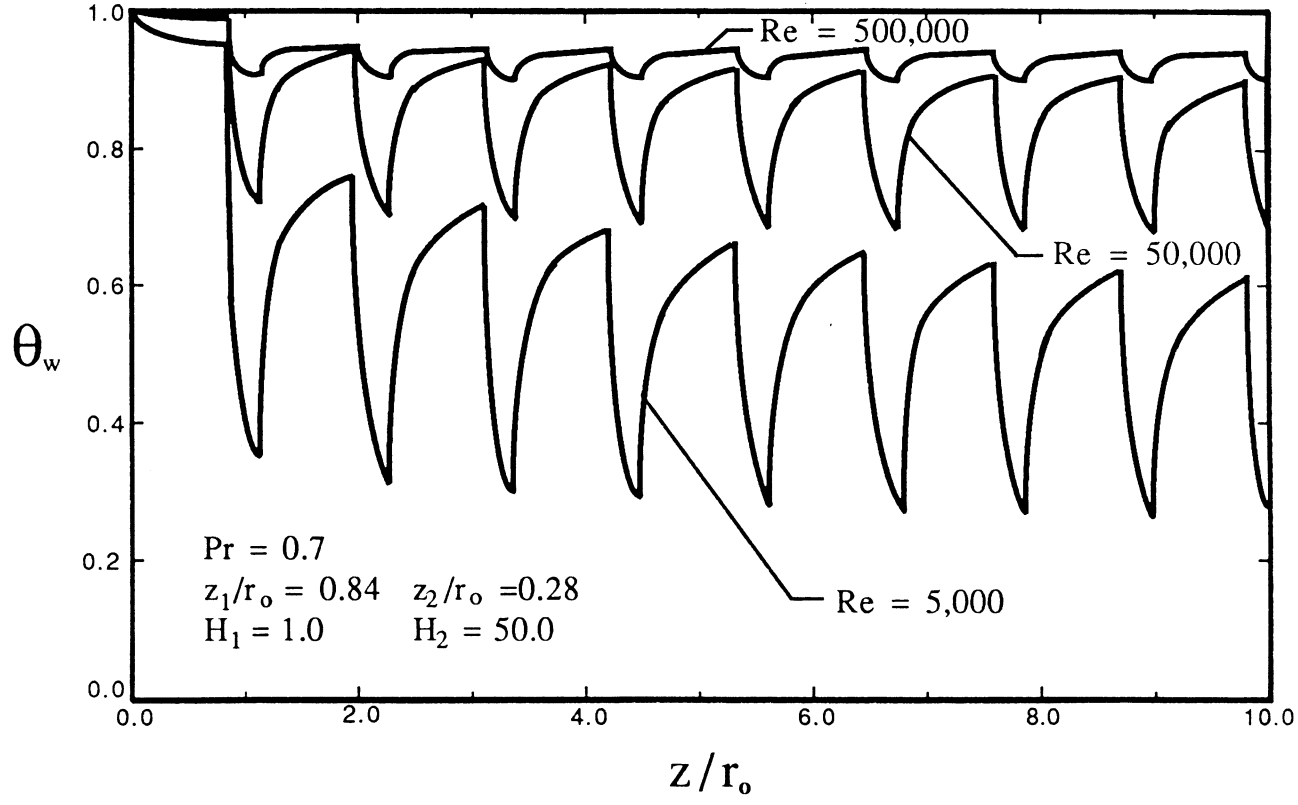

Figure 12. Wall temperature results showing the effect of Re for a stepwise periodic heat transfer coefficient in turbulent pipe flow

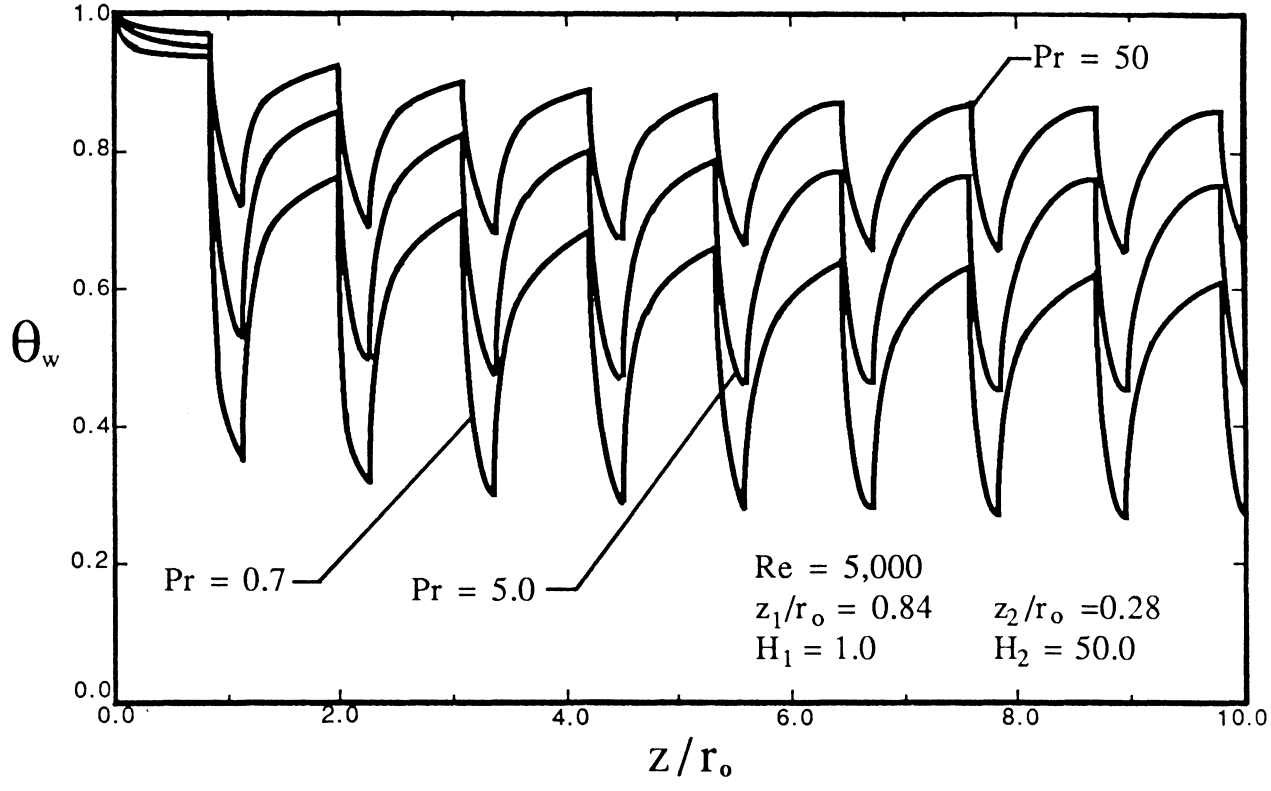

Figure 13. Wall temperature results showing the effect of Pr for a stepwise periodic heat transfer coefficient in turbulent pipe flow

$$\frac{g(\eta)}{RePr} = \frac{1}{Re}\left[\frac{1}{Pr} + \frac{1}{Pr_t}\frac{\varepsilon_m}{\nu}\right] \tag{31}$$

Now, it is clear that the radial heat transfer is made up of both a molecular diffusion term, represented by $\frac{1}{Pr}$, and a turbulent mixing term, represented by $\frac{\varepsilon_m}{\nu Pr_t}$, acting in parallel. At small Pr, the results appear similar to those of laminar flow because a large thermal diffusivity makes molecular effects important, as seen from Eq. (31). As Pr is increased, the effects of turbulent mixing begin to dominate the molecular diffusion and, consequently, the wall temperature is much higher in this case. As in Fig. 12, the wall temperature falls into a repetitive pattern with an ever-decreasing magnitude as heat is given up to the surroundings.

The remaining figures present results in terms of the dimensionless heat transfer, Q as given by Eq. (29), which is a meaningful way to display the enhancement of the heat transfer due to external finning.

Figure 14 shows the total heat transfer for fully developed laminar flow in a pipe for stepwise and harmonic variations of the Biot number. The constant H case, $H(\xi) = 1$, represents a tube with no enhancement. On the log scale used in Fig. 14, the abrupt changes caused by the stepwise periodic variation in the Biot number are clearly shown. Both the stepwise and the harmonic variations of the Biot number provide a significant degree of enhancement over the constant Biot case, with the harmonic variation being the most efficient. Thus, for heat exchange equipment where precise performance calculations or optimization is critical, an analysis coupling the fluid with the

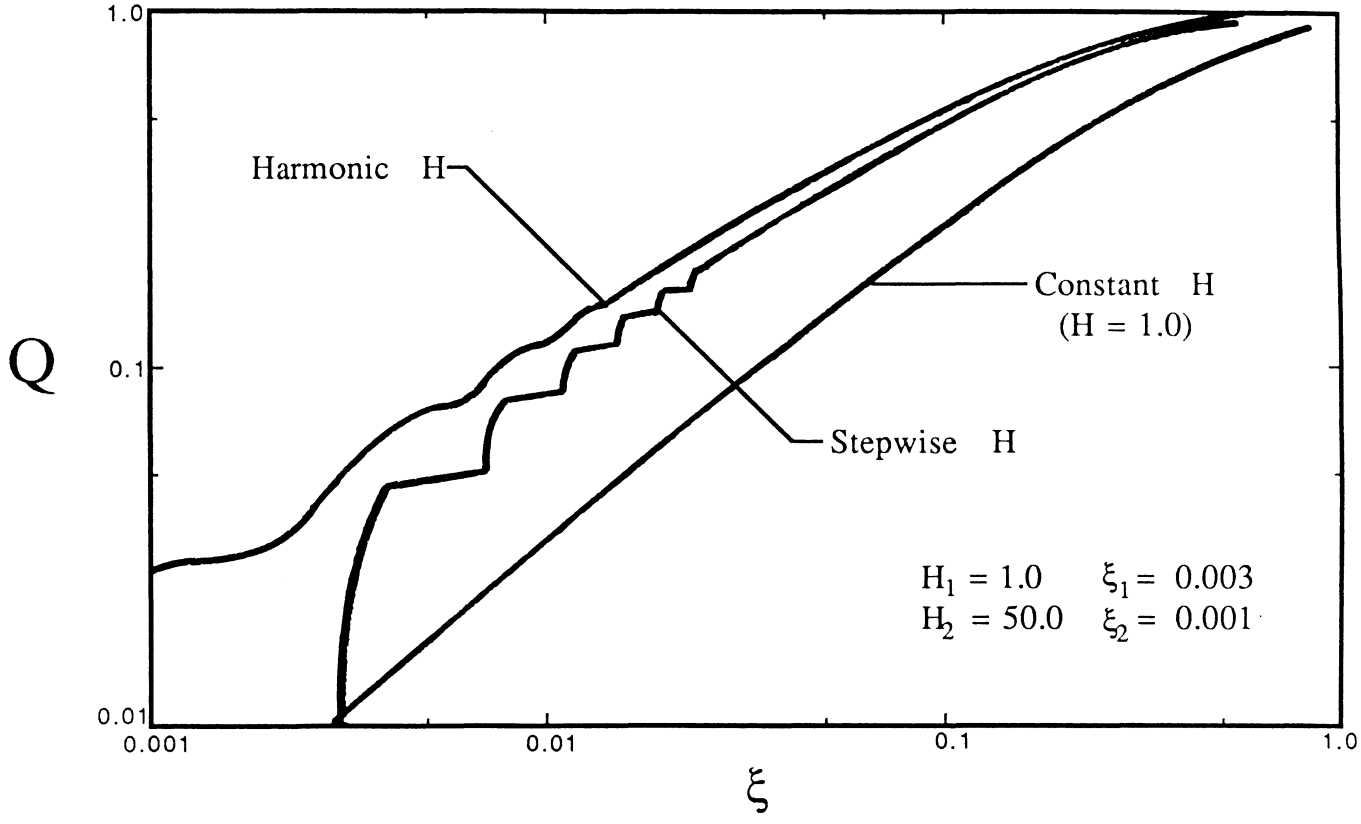

Figure 14. Total heat transfer results showing the effect of the convection coefficient on laminar pipe flow

conduction in the wall and fin could be warranted.

In Fig. 15, the total heat transfer for turbulent pipe flow is presented. Again, the constant H case represents an unfinned tube. The results of Fig. 15 are qualitatively similar to those of Fig. 14, except that in turbulent flow, the exact variation of the Biot number does not appear to be as significant as in laminar flow.

Figure 16 shows the effect of the interfin spacing on the total heat transfer in laminar flow. Clearly, the more often the fluid is subjected to regions of high H, the faster it will give up its heat to the surroundings. Thus, the larger the interfin spacing the longer it will take to cool the fluid. Here, the case $\xi_1 = \infty$ represents an unfinned tube.

Figure 17 shows the effect of interfin spacing for a turbulent pipe flow. Again, the closer the fins are placed, the more heat can be transferred from the fluid. In actuality, of course, the external convection coefficient is dependent on the interfin spacing, since the fluid flow between the fins creates the convective environment. This effect has not been included here, but could warrant consideration.

In Fig. 18, the effect of Re on the rate of heat transfer from the pipe is examined. Here, the lower Re flow approaches thermal saturation by 250 pipe diameters. A tenfold increase in Re requires almost ten times the pipe length to achieve thermal saturation. The effect of greater mixing in the higher Re flows, however, allows the fluid to transfer heat faster to the wall, thus reducing the length of pipe required. The effect of Pr on the total heat transfer rate can be seen in Fig. 19. The total heat transfer increases as Pr is decreased due to

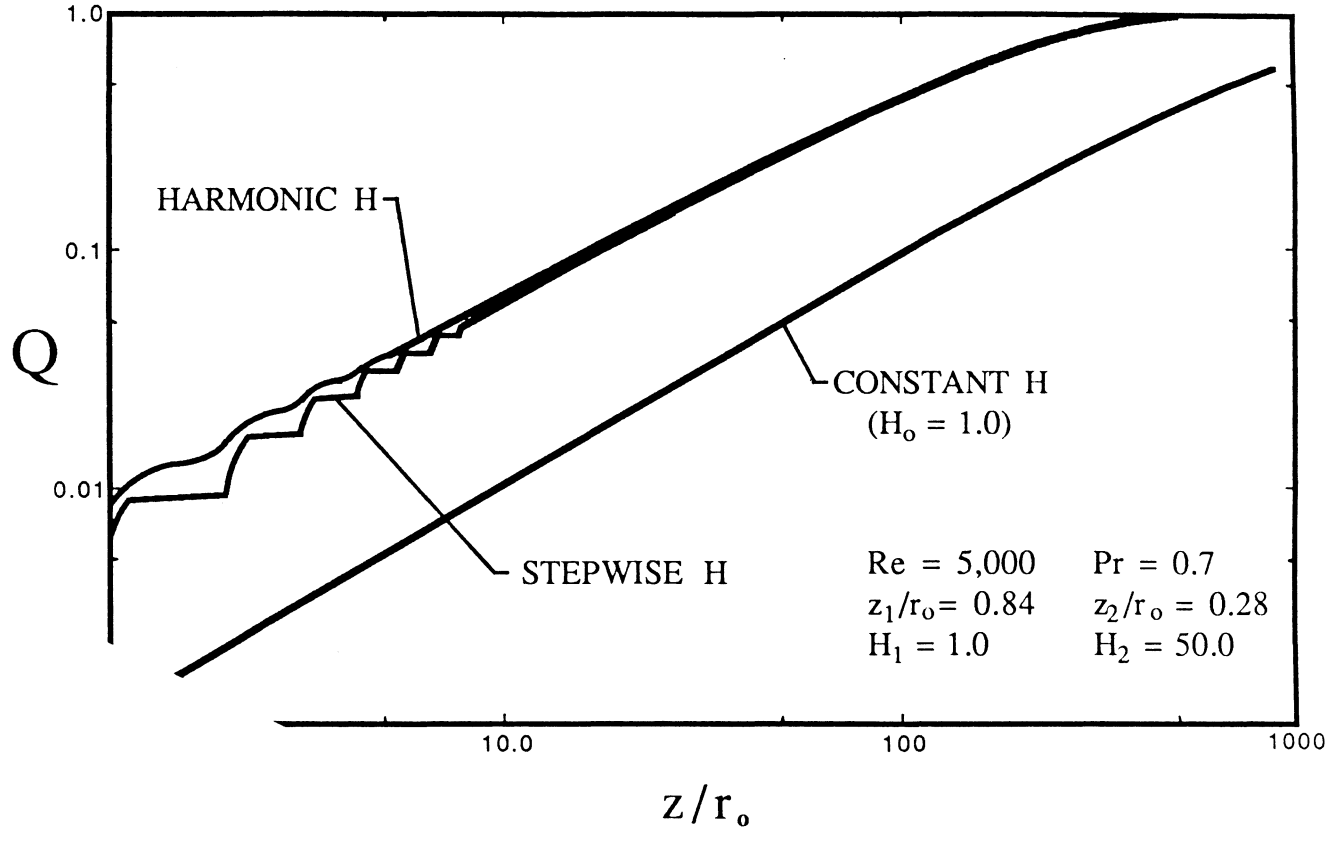

Figure 15. Total heat transfer results showing the effect of the convection coefficient on turbulent pipe flow

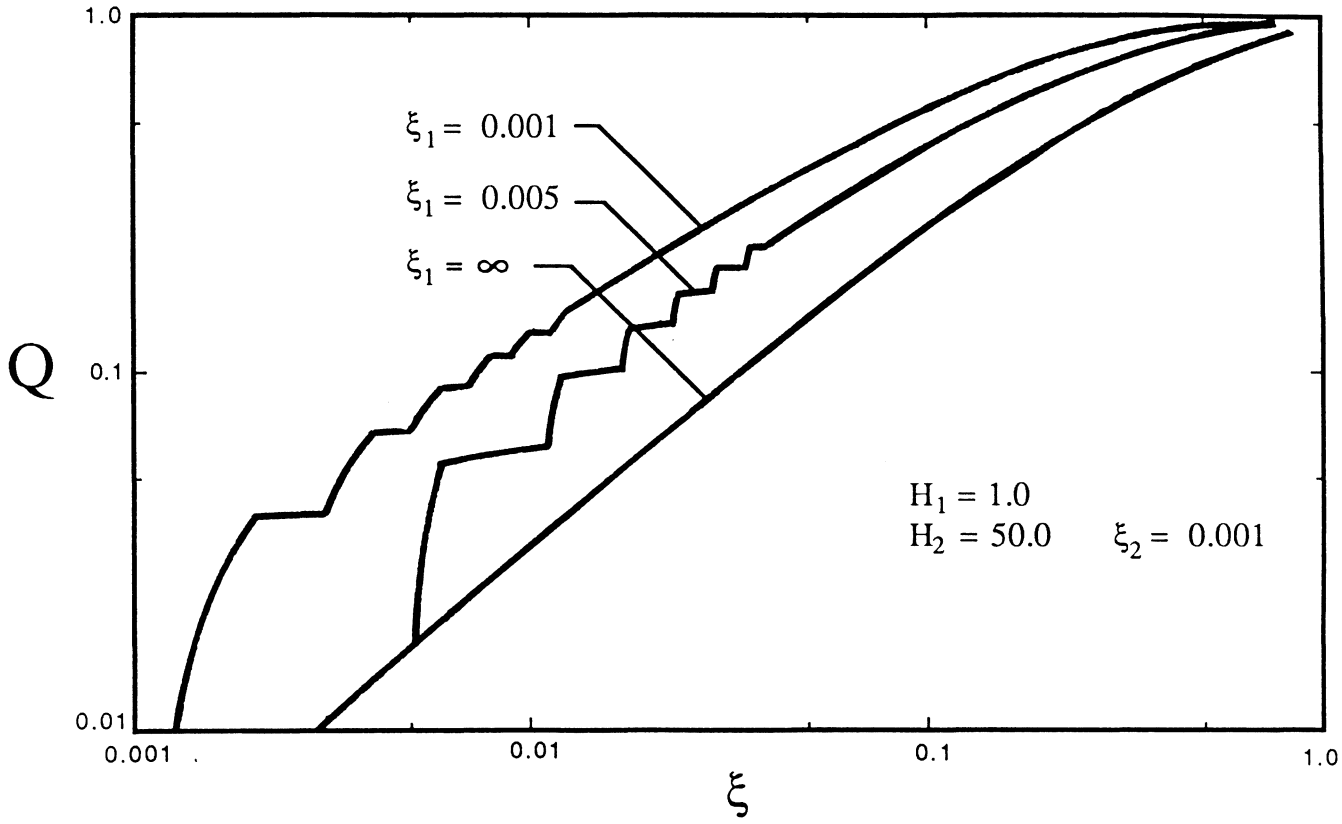

Figure 16. Total heat transfer results showing the effect of interfin spacing on laminar pipe flow

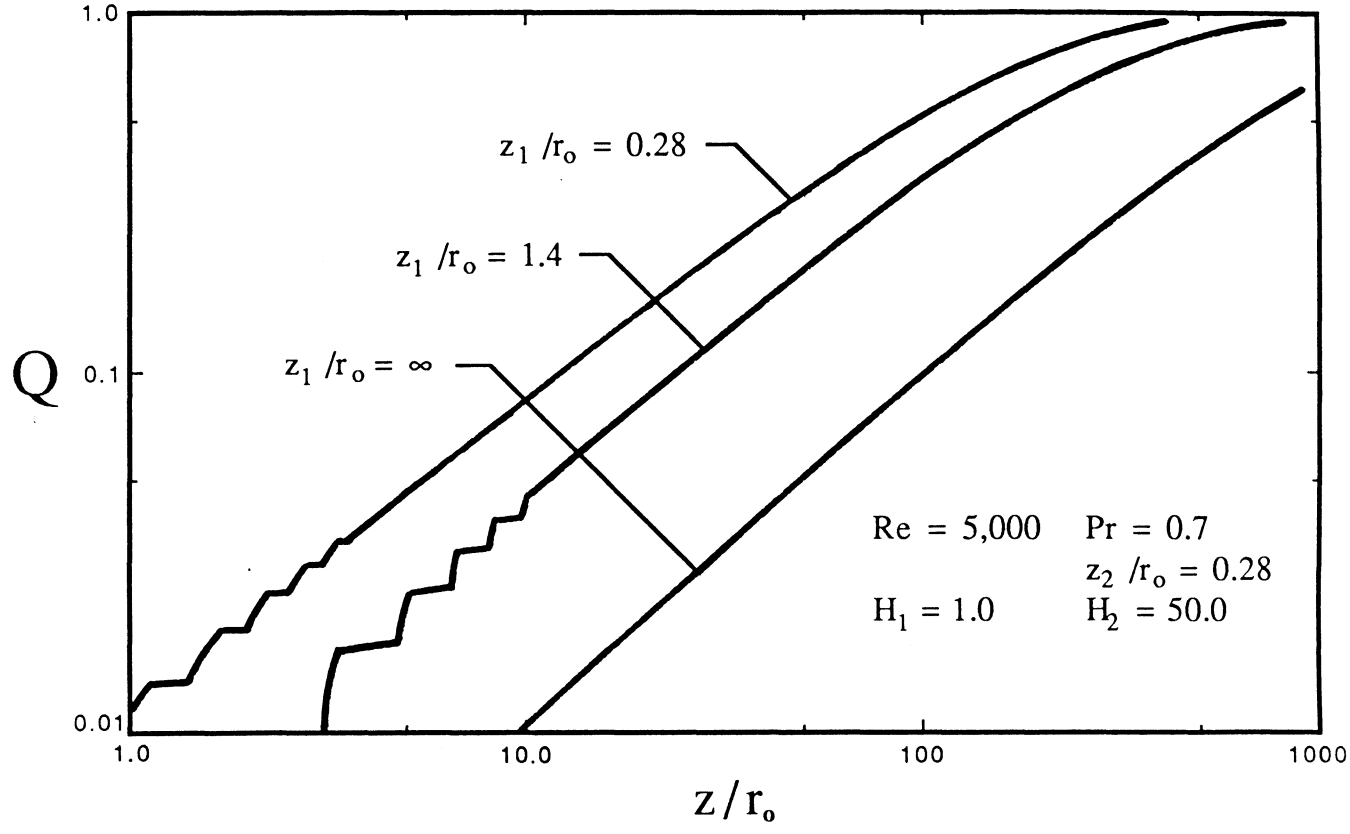

Figure 17. Total heat transfer results showing the effect of interfin spacing on turbulent pipe flow

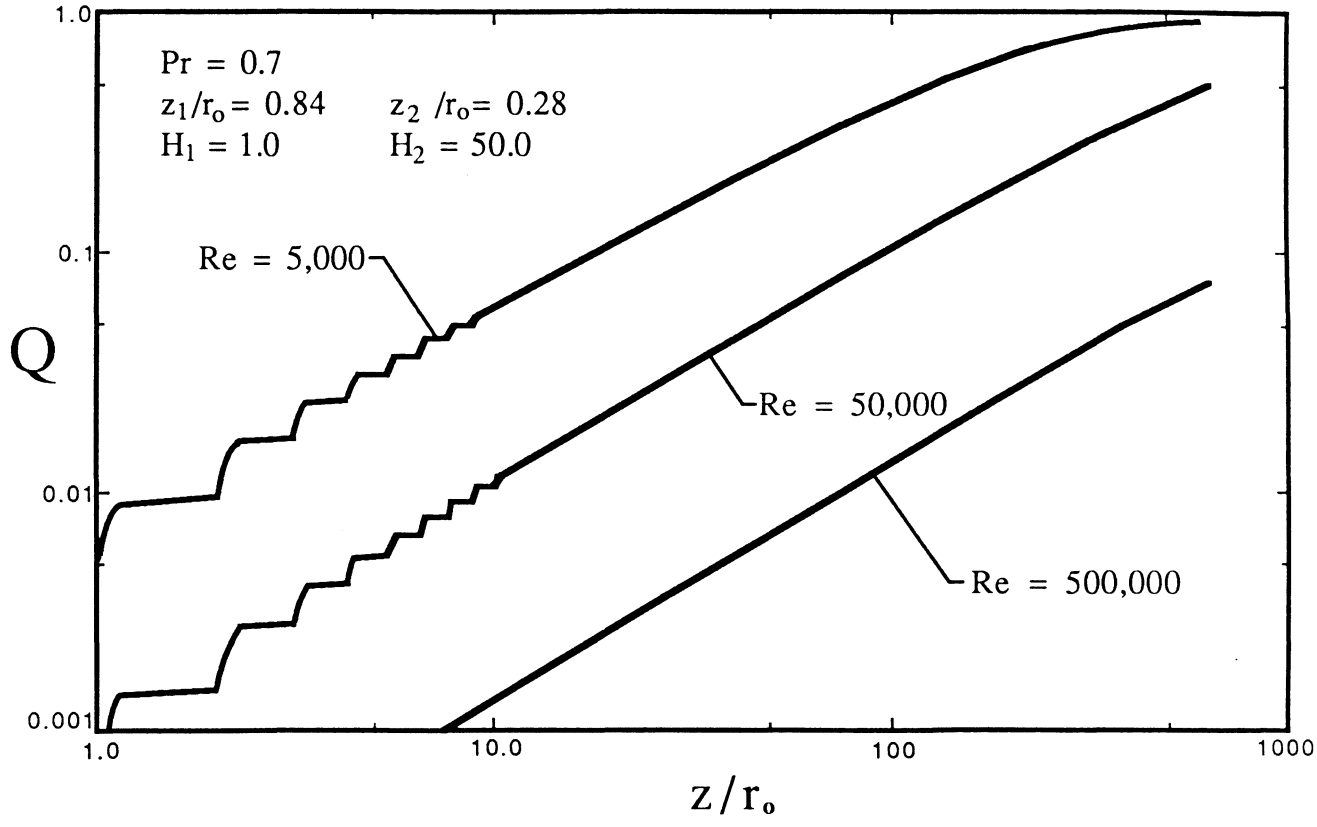

Figure 18. Total heat transfer results showing the effect of Re on turbulent pipe flow

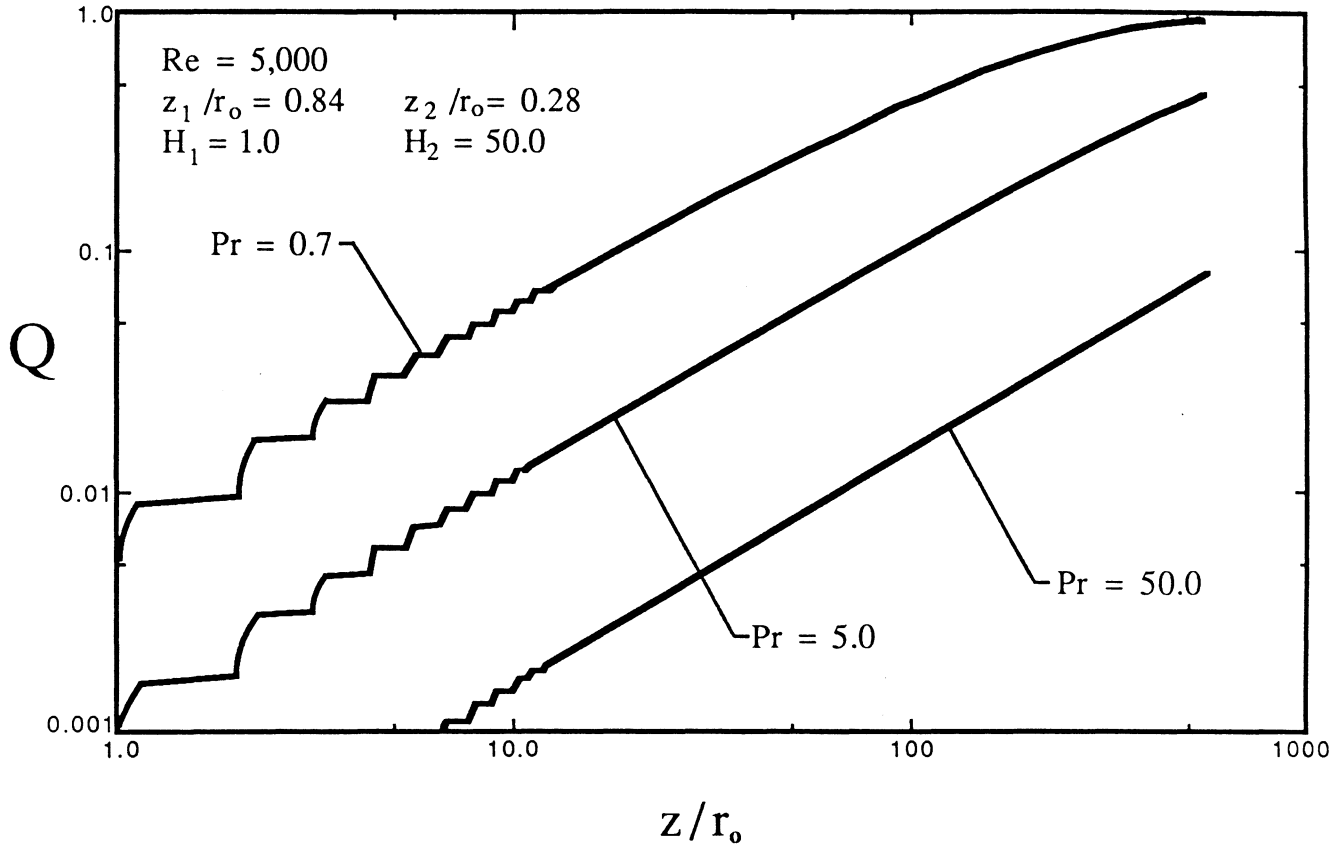

Figure 19. Total heat transfer results showing the effect of Pr on turbulent pipe flow

an increase in the molecular portion of the total thermal diffusivity.

Figure 20 presents a comparison of the heat transfer rates of slug and laminar tube flow. The results appear qualitatively similar for both cases, with slug flow transferring heat faster due to a higher velocity near the wall.

The effect of the flow model on the total heat transfer is examined in Fig. 21. It has been assumed that laminar flow can be maintained up to a Re of 4,000. Hinze [57, p. 707] reports that when particular care is taken, laminar flow can be maintained up to Re = 10^5. As expected, laminar flow provides the greatest resistance to heat transfer because of a low velocity near the wall and the absence of any mixing effects. Perhaps not so expected is the fact that slug flow gives higher heat transfer rates than turbulent flow up to about 30 diameters, after which turbulent flow achieves higher heat transfer rates. Apparently, the high velocity near the wall dominates the heat transfer characteristics when the bulk temperature is large. Eventually, however the effect of turbulent mixing overtakes the effect of high wall velocity and the turbulent heat transfer becomes greater.

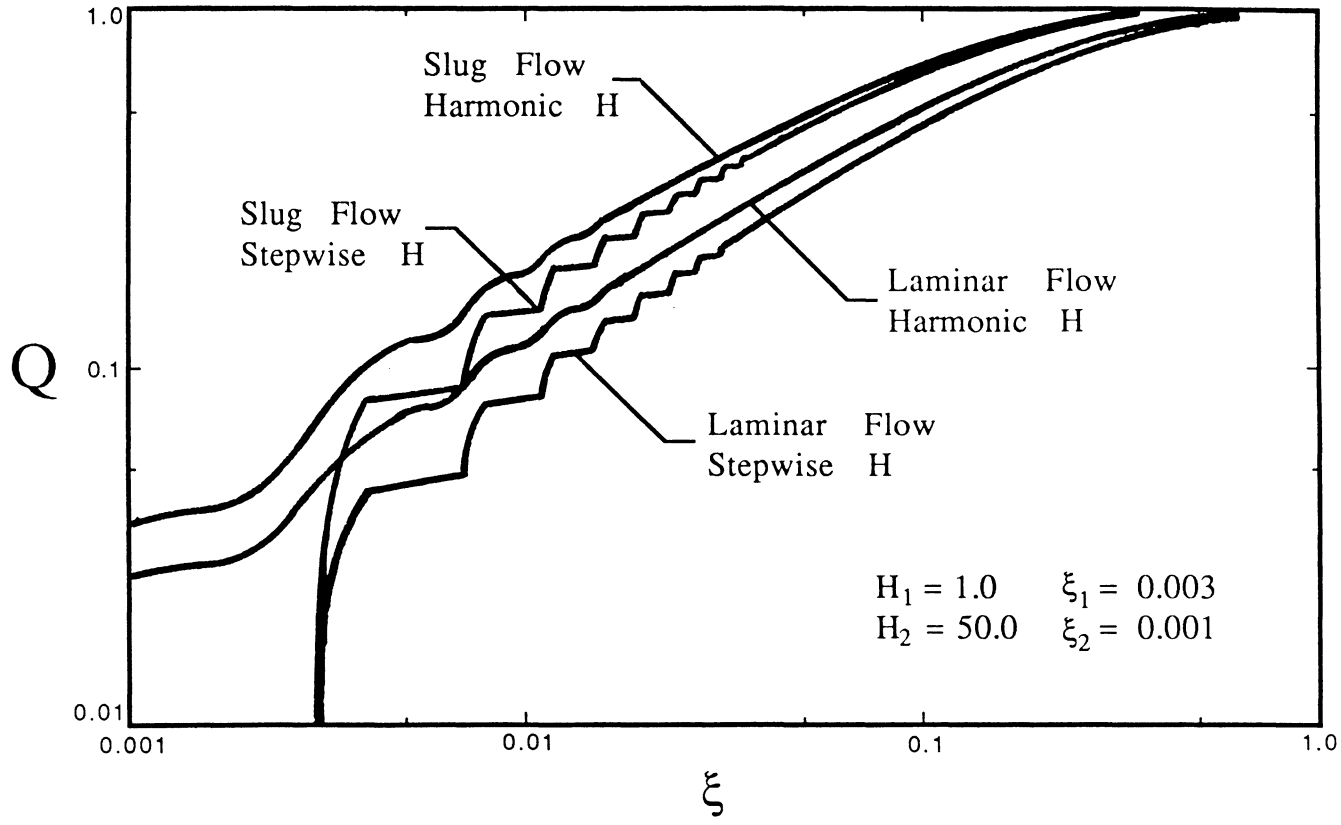

Figure 20. Total heat transfer results showing the effect of the velocity profile and convection coefficient

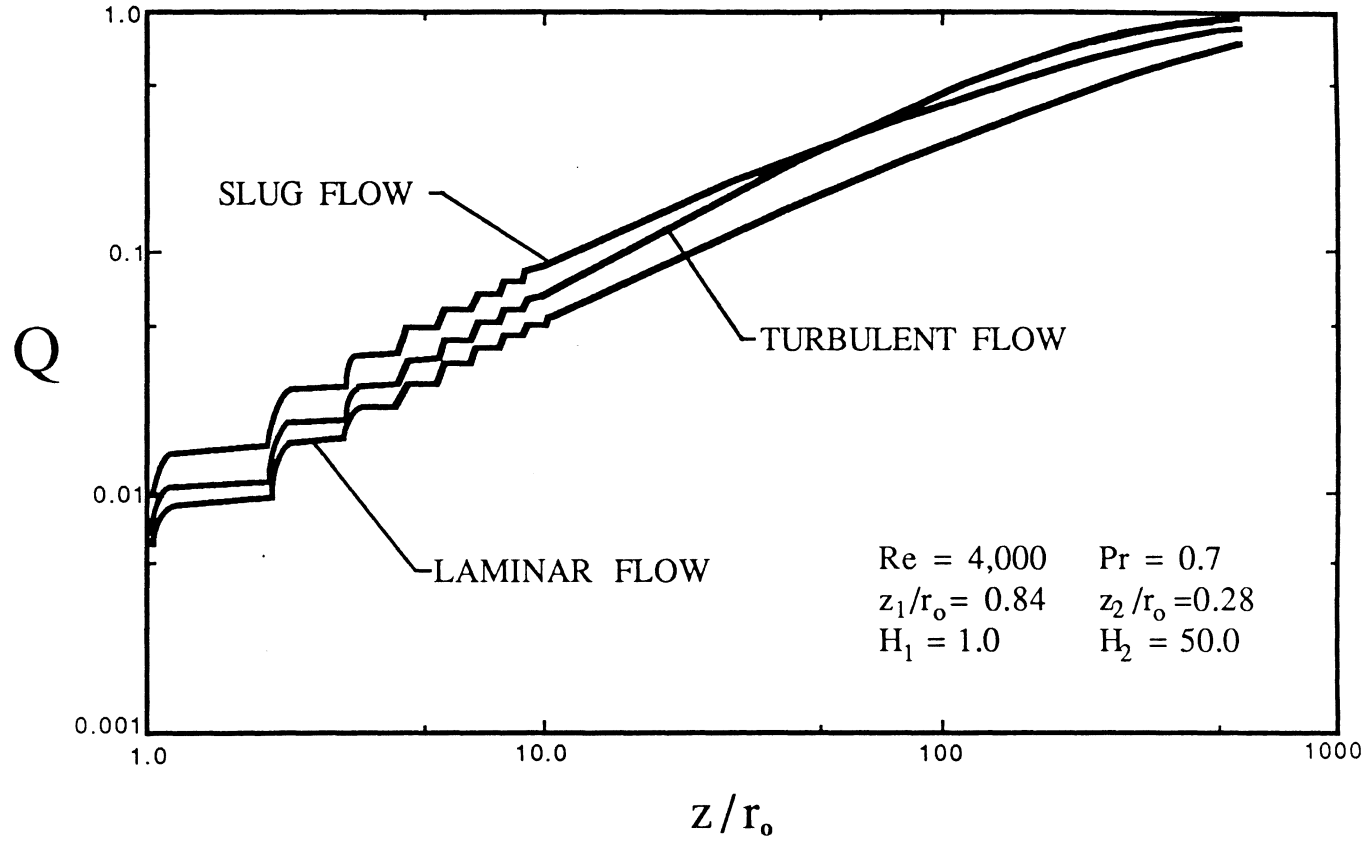

Figure 21. Total heat transfer results showing the effect of the flow model for a stepwise periodic heat transfer coefficient

VI. SUMMARY AND CONCLUSIONS

This investigation presents a solution methodology to solve the problem of a fully developed internal flow subjected to an axial variation of the heat transfer coefficient. The solution is developed in terms of a fully developed turbulent flow and is shown to contain the solutions for slug and laminar flow as special cases. The generalization to a variable heat transfer coefficient causes mathematical complexities due to the nonseparable nature of the problem. The solution technique uses Green's functions to derive a singular Volterra integral equation for the temperature of the fluid at the wall. The integral equation is resolved through numerical integration with the aid of a singularity subtraction procedure.

Before considering the solutions of the integral equation, a thorough examinaton is made of each of the building blocks needed in the solution procedure. The most basic elements required are the dimensionless velocity profile and the dimensionless total diffusity. A comparison is made of the eigenvalue problems for each of the three cases considered through an exmaination of the normalized eigenfunctions and the eigenvalues, which are required to form the Green's function. A consideration of the respective Green's functions is given showing the effect of the parameters, Re, Pr and H_o on the singular nature of the Green's function.

Results are presented for both a stepwise periodic and a harmonic variation of the external convection coefficient for slug, laminar and turbulent pipe flow. In each case, the harmonic variation of the Biot number produces higher heat transfer rates than the stepwise periodic

variation with equal averages. However, the difference is only appreciable at a high degree of enhancement, (H_2/H_1 large) and when the internal resistance is high (laminar flow). The exact variation of the Biot number does not appear to be important when the degree of enhancement is low as long as the average value remains the same. An analysis showing when the constant average Biot number approximation can be applied to a finned tube is presented in Wells [62]. In all cases, the wall temperature is very sensitive to the Biot number variation. In turbulent pipe flow, an increase in Re or Pr results in higher wall temperatures, and smaller heat transfer rates. A comparison of the heat transfer rates for the three flow models shows that laminar flow has the highest internal resistance due to a low velocity near the wall and the absence of turbulent mixing effects. The slug flow model gives the highest heat transfer rates near the inlet of the pipe due to the high wall velocity, however, the heat transfer in the turbulent case eventually overtakes the slug flow case due to the turbulent mixing effects.

In this investigation, attention is focused on heat transfer from a tube with negligible wall thickness by virtue of an axial variation of the heat transfer coefficient for fully developed internal flow. Thus, the results provide no insight into the effect of heat conduction in the wall, the effect of a developing velocity profile, or the effect of an angular variation of the heat transfer coefficient. In practice, of course, each of these effects is present and, clearly, further work is needed to determine their relative importance.

Overall, the solution technique has proven to be both accurate and economical, by combining the advantages of an analytical formulation

with a simple numerical integration. The methodology itself is quite general and can handle a large class of problems with variable boundary condition parameters.

References

1. Travis, J. R., Buhr, H. O., and Sesonske, A., "A Model for Velocity and Eddy Diffusivity Distributions in Fully Turbulent Pipe Flow," Canadian Journal of Chemical Engineering, Vol. 49, 1971, pp. 14-18.

2. Sparrow, E. M., and Charmchi, M., "Laminar Heat Transfer in an Externally Finned Circular Tube," Journal of Heat Transfer, Vol. 102, 1980, pp. 605-611.

3. Vick, B., and Wells, R. G., "Laminar Flow with an Axially Varying Heat Transfer Coefficient," Int. J. Heat Mass Transfer, Vol. 29, 1986, pp. 1881-1889.

4. Graetz, L., "Uber die Warmeleitungsfahigheit von Flussigkeiten," Annalen de Physik und Chemie, Vol. 25, 1885, pp. 337-357.

5. Shah, R. K., and London, A. L., Laminar Flow Forced Convection in Ducts, Academic Press, New York, 1978.

6. Siegel, R., Sparrow, E. M., and Hallman, T. M., "Steady Laminar Heat Transfer in a Circular Tube with Prescribed Wall Heat Flux," Applied Scientific Research, Vol. A7, 195B, pp. 386-392.

7. Hsu, C. J., "Laminar Flow Heat Transfer in Circular or Parallel Plate Channels with Internal Heat Generation and Boundary Conditions of the Third Kind," Journal of the Chinese Institute of Chemical Engineering, Vol. 2, 1971, pp. 85-100.

8. Mitchell, J. W., "An Expression for Internal Flow Heat Transfer for Polynomial Wall Temperature Distribution," Journal of Heat Transfer, Vol. 91, 1969, pp. 175-177.

9. Shapovalov, V. V., "Heat Transfer in Laminar Flow of an Incompressible Fluid in a Round Tube," Journal of Engineering Physics (USSR), Vol. 12, 1967, pp. 363-364.

10. Zaychik, L. I., "Application of the Laplace Transformation to the Problem of Heat Transfer in a Tube with Variable Boundary Conditions," Heat Transfer Soviet Research, Vol. 11, 1979, pp. 101-106.

11. Chandler, R. D., Panaia, J. N., Stevens, R. B., and Zinsmeister, G. E., "The Solution of Steady State Convection Problems by the Fixed Random Wall Method," Journal of Heat Transfer, Vol. 90, 1968, pp. 361-363.

12. Tay, A. O., and De Vahl Davis, G., "Application of the Finite Element Method to Convection Heat Transfer Between Parallel Plates," Int. J. Heat Mass Transfer, Vol. 14, 1971, pp. 1057-1069.

13. Casarella, M. J., Laura, P. A., and Chi, M., "On the Approximate Solution of Flow and Heat Transfer Through Non-Circular Conduits with Uniform Wall Temperature," British Journal of Applied Physics, Vol. 18, 1967, pp. 1327-1335.

14. Povarnitsyn, M. S., and Yurlova, E. V., "Calculation of the Temperature Field in a Plane Channel with Non-uniform Heating of Thermally Conducting Walls," Journal of Engineering Physics (USSR), Vol. 10, 1966, pp. 82-85.

15. Savkar, S. D., "On a Variational Formulation of a Class of Thermal Entrance Problems," Int. J. Heat Mass Transfer, Vol. 13, 1970, pp. 1187-1197.

16. Boussinesq, J., "Theorie de l'ecoulement Toubillant," Mem. Pres. par div. Savant a L'acad. Sci. Paris, Vol. 23, 1877, p. 46.

17. Prandtl, L., "Uber die Ausgebildete Turbulenz," ZAMM, Vol. 5, 1925, pp. 136-139.

18. Deissler, R. G., "Analysis of Turbulent Heat Transfer, Mass Transfer and Friction in Smooth Tubes at High Prandtl and Schmidt Numbers," NASA Report 1210, Washington, DC, 1955.

19. Riechardt, H. A., "Vollstandige Darstellung der Turbulenten Geschwindigkeitsverteilung in Glatten Leitungen," ZAMM, Vol. 31, 1951, pp. 208-219.

20. Martinelli, R. C., "Heat Trasnfer to Molten Metals," Transactions of ASME, Vol. 69, 1947, pp. 947-959.

21. Sleicher, C. A., and Tribus, M., "Heat Transfer in a Pipe with Turbulent Flow and Arbitrary Wall Temperature Distribution," Transactions of ASME, Vol. 79, 1957, pp. 789-797.

22. Sleicher, C. A., Notter, R. H., and Crippen, M. D., "A Solution to the Turbulent Graetz Problem by Matched Asymptotic Expansions - I: The Case of Uniform Wall Temperature," Chemical Engineering Science, Vol. 25, 1970, pp. 845-857.

23. Notter, R. H., and Sleicher, C. A., "A Solution to the Turbulent Graetz Problem by Matched Asymptotic Expansions - II: The case of Uniform Wall Heat Flux," Chemical Engineering Science, Vol. 26, 1971, pp. 559-565.

24. Notter, R. H., and Sleicher, C. A., "A Solution to the Turbulent Graetz Problem - III: Full Developed and Entry Region Heat Transfer Rates," Chemical Engineering Science, Vol. 27, 1972, pp. 2073-2093.

25. Shibani, A. A., and Ozisik, M. N., "A Solution to Heat Transfer in Turbulent Flow between Parallel Plates," Int. J. Heat Mass Transfer, Vol. 20, 1977, pp. 565-573.

26. Bergles, A. E., Brown, G. S., Jr., and Snider, W. D., "Heat Transfer Performance of Internally Finned Tubes," ASME Paper No. 71-HT-31, 1971.

27. Bergles, A. E., "Survey and Evaluation of Techniques to Augment Convective Heat and Mass Transfer," Progress in Heat and Mass Transfer, Vol. 1, Pergamon Press, 1969, pp. 331-424.

28. Gardner, K. A., "Efficiency of Extended Surface," Transactions of ASME, Vol. 67, 1945, pp. 621-631.

29. Harper, D. R. and Brown, W. B., "Mathematical Equations for Heat Conduction in the Fins of Air-Cooled Engines," NACA Report 158, 1922.

30. Razelos, P., "The Optimum Dimensions of Convective Pin Fins," Journal of Heat Transfer, Vol. 150, 1983, pp. 411-413.

31. Kovarik, M., "Optimal Heat Transfer Assemblies with Thin, Straight Fins," Journal of Heat Transfer, Vol. 105, 1983, pp. 203-205.

32. Razelos, P., and Imre, K., "The Optimum Dimensions of Circular Fins with Variable Thermal Parameters," Journal of Heat Transfer, Vol. 102, 1980, pp. 420-425.

33. Poulikakos, D., and Bejan, A., "Fin Geometry for Minimum Entropy Genration in Forced Convection," Journal of Heat Transfer, Vol. 104, 1982, pp. 616-623.

34. Guceri, S., and Maday, C. J., "A Least Weight Circular Cooling Fin," Journal of Engineering for Industry, Vo. 97, 1975, pp. 1190-1193.

35. Mikhailov, M. D., "On the Solution of the Heat Equation with Time Dependent Coefficient," Int. J. Heat Mass Transfer, Vol. 18, 1975, pp. 344-345.

36. Ozisik, M. N., and Murray, R. L., "On the Solution of Linear Diffusion Problems with Variable Boundary Condition Parameters," Journal of Heat Transfer, Vol. 96, 1974, pp. 48-51.

37. Ivanov, V. V., and Salomatov, V. V., "On the Calculation of the Temperature Field in Solids with Variable Heat Transfer Coefficients," Inzhenerno-Fizicheskii Zhurnal, Vol. 9, 1965, pp. 83-85.

38. Thompson, J. J., and Holy, Z. J., "Axisymmetric Thermal Response Problems for a Spherical Fuel Element with Time-dependent Heat Transfer Coefficients," Nuclear Engineering and Design, Vol. 9, 1969, pp. 29-44.

39. Holy, Z. J., "Temperature and Stresses in Reactor Fuel Elements Due to Time- and Space-dependent Heat Transfer Coefficients," Nuclear Engineering and Design, Vol. 18, 1972, pp. 145-197.

40. Reed, J. R., and Mullineux, G., "Quasi-Steady State Solution of Periodically Varying Phenomena," Int. J. Heat Mass Trans. Vol. 16, 1973, pp. 2007-2012.

41. Mikhailov, M. D., "Quasi-Steady State Temperature Distribution in Finite Regions with Periodically Varying Boundary Conditions," Int. J. Heat Mass Transfer, Vol. 17, 1974, pp. 1475-1478.

42. Vick, B., and Ozisik, M. N., "Quasi-Steady Stae Temperature Distribution in Periodically Contacting Finite Regions," Journal of Heat Transfer, Vol. 103, 1981, pp. 739-744.

43. Ozisik, M. N., and Guceri, S. I., "A Variable Eigenvalue Approach to Phase Change Problems," Canadian Journal of Chemical Engineering, Vol. 55, 1977, pp. 145-148.

44. Hochstadt, H., Integral Equations, John Wiley and Sons, New York, 1973.

45. Tricomi, F. G., Integral Equations, Interscience, New York, 1957.

46. Muskhelishvili, N. I., Singular Integral Equations, Noordhoff, Holland, 1953.

47. Brunner, H., "Survey of Recent Advances in the Numerical Treatment of Volterra Integral and Integrodifferential Equations," J. Comp. Appl. Math., Vol. 8, 1982, pp. 213-229.

48. Brunner, H., and te Riele, H. J. J., "Volterra-type Integral Equations of the Second Kind wtih Non-smooth Solutions: High-order Methods Based on Collocation Techniques," Journal of Integral Equations, Vol. 6, 1984, pp. 187-203.

49. Bownds, J. M., "A Combined Recursive Collocation and Kernel Approximation Technique for Certain Singular Volterra Integral Equations," Journal of Integral Equations, Vol. 1, 1979, pp. 153-164.

50. Linz, P., "Numerical Methods for Volterra Integral Equations with Singular Kernels," SIAM J. Numer. Anal., Vol. 6, 1969, pp. 365-374.

51. Garey, L., "Numerical Solution of Volterra Integral Equations with Singular Kernels," BIT, Vol. 14, 1974, pp. 33-39.

52. Bownds, J. M., and Wood, B., "A Smoothed Projection Method for Singular, Nonlinear Volterra Integral Equations," J. Approx. Theory, Vol. 25, 1979, pp. 120-141.

53. te Riele, H. J. J., "Collocation Methods for Weakly Singular Second Kind Volterra Integral Equations with Nonsmooth Solution," IMA J. Numer. Anal., Vol. 2, 1982, pp. 437-449.

54. El Tom, M. E. A., "Spline Function Approximations to the Solution of Singular Volterra Integral Equations of the Second Kind," J. Inst. Math. Applics., Vol. 14, 1974, pp. 303-309.

55. Monin, A. S. and Yaglom, A. M., Statistical Fluid Mechanics: Mechanics of Turbulence, MIT Press, Cambridge, Massachusetts, 1971, Ch. 3.

56. Cebeci, T., "A Model for Eddy Conductivity and Turbulent Prandtl Number," Journal of Heat Transfer, Vol. 95, 1973, pp. 227-234.

57. Hinze, J. O., Turbulence, McGraw-Hill, New York, 1975.

58. Lauwerier, H. A., "The Use of Confluent Hypergeometric Functions in Mathematical Physics and the Solution of an Eigenvalue Problem," Applied Scientific Research, Vol. A2, 1959, pp. 184-204.

59. Lauwerier, H. A., "Poiseuille Function," Applied Scientific Research, Vol. A3, 1951, pp. 58-72.

60. Ozisik, M. N., Heat Conduction, John Wiley and Sons, New York, 1980, Chapter 13.

61. Kleinman, R. E., "Some Applications of Functional Analysis in Classical Scattering," Mathematical Methods and Applications of Scattering Theory, Springer-Verlag, Berlin, 1980.

62. Wells, R. G., "Laminar Flow with an Axially Varying Heat Transfer Coefficient," Masters Thesis, Virginia Polytechnic Institute and State University, 1986.

63. James, M. L., Smith, G. M., and Wolford, J. G., Applied Numerical Methods for Digital Computation, Harper and Row, New York, 1977.

64. Delves, L. M., and Mohamed, J. L., Computational Methods for Integral Equations, Cambridge University Press, New York, 1985.

65. Incropera, F. P. and DeWitt, D. P., Fundamentals of Heat Transfer, John Wiley and Sons, New York, 1981, Chapter 8.

66. Rabenstein, A. L., Introduction to Ordinary Differential Equations, Academic Press, New York, 1972, pg. 262.

APPENDIX A: Eigenvalue Problems

The appropriate form of the eigenvalue problem is obtained from the homogeneous, separated version of the system of Eqs. (19). The result is

$$\frac{d}{d\eta}\left[\eta^i g(\eta)\frac{d\psi_m}{d\eta}\right] + \lambda_m^2 \eta^i \frac{v(\eta)}{2}\psi_m(\eta) = 0 \tag{A1a}$$

$$\begin{aligned} &\frac{d\psi_m}{d\eta} = 0 \quad , \quad \eta = 0 \ (i = 0) \\ &\psi_m, \frac{d\psi_m}{d\eta} \text{ finite} \ , \ \eta \to 0 \ (i = 1) \end{aligned} \tag{A1b}$$

$$\frac{d\psi_m}{d\eta} + H_o\psi_m = 0 \quad , \quad \eta = 1 \tag{A1c}$$

When $i = 0$ (parallel plates), the Sturm-Liouville system (A1) is self-adjoint with the symmetry condition $\frac{d\psi_m}{d\eta} = 0$. However, when $i = 1$ (circular tube) the Sturm-Liouville system (A1) is singular since the leading coefficient $\eta g(\eta)$ vanishes at $\eta = 0$. In this case, the conditions on the finiteness of the eigenfunction and its derivative are required to ensure that the differential equation (A1a) is self-adjoint [66].

The eigenfunctions are normalized so that

$$\int_{\eta=0}^{1} \eta^i \frac{v(\eta)}{2}\psi_m^2(\eta)\, d\eta = 1 \tag{A2}$$

With all the different combinatons of geometry and flow, the eigenvalue problem (A1) represents six separate eigenvalue problems.

However, solutions are only presented here for the cases of slug flow in a tube, laminar flow in a tube and turbulent flow in a tube.

The eigenvalue problem with i = 1, v(η) = 1 and g(η) = 1 yields the well-known Bessel functions. The eigenfunctions are given by

$$\psi_m(\eta) = J_o\left(\frac{\lambda_m}{\sqrt{2}} \eta \right) / \sqrt{N_m} \tag{A3}$$

The eigenvalues are the positive roots of the following transcendental equation,

$$J_o\left(\frac{\lambda_m}{\sqrt{2}} \right) H_o = \frac{\lambda_m}{\sqrt{2}} J_1\left(\frac{\lambda_m}{\sqrt{2}} \right) \tag{A4}$$

The normalization integral is given by,

$$N_m = \frac{J_o^2 \left(\frac{\lambda_m}{\sqrt{2}} \right)\left(H_o^2 + \frac{\lambda_m^2}{2} \right)}{\lambda_m^2} \tag{A5}$$

The second eigenvalue problem of interest occurs if i = 1, v(η) = $2(1 - \eta^2)$ and g(η) = 1. This is the well-known Graetz problem which has been studied by numerous workers with varying degrees of success. As described in reference [62], there are two distinct solution techniques, one for the small eigenvalues and another for the large eigenvalues. The first method, accurate for the first fifteen eigenvalues, involves conversion of the eigenvalue problem into the form of a confluent hypergeometric equation from which a series solution is developed. The second method, accurate from the fifth eigenvalue onward, is due to Lauwerier [58,59]. With this technique, the eigenvalue problem is

converted into the confluent hypergeometric form and then developed into an asymptotic sequence with the WKB method. The formulas necessary for the calculation of the eigenvalues, eigenfunctions and norms are presented in reference [62] along with the program used to calculate them.

The final eigenvalue problem considered here occurs for turbulent flow in a tube. In this case, $i = 1$, $g(\eta)$ is given by equations (15g), (18a,b) and Table 1 and the velocity profile is obtained by numerical integration of equation (16d). Although the eigenvalue problem might be solved by the method of matched asymptotic expansions for simple forms of the eddy diffusivity and velocity as reported in references [20-25], the numerically integrated velocity profile in this case makes such an approach impractical. For this reason, the eigenvalue problem was solved numerically using an iterative approach with Butcher's (5,6) Runge-Kutta algorithm [63]. A "shooting method" is adopted with the boundary condition at $\eta = 1$ providing the convergence criteria, since if λ_m is chosen precisely, then the boundary condition will be exactly satisfied.

APPENDIX B: Green's Function

A necessary ingredient to the solution of the integral equation (22) is the Green's function itself, as governed by the system of equations (19). As mentioned in the text, this set of equations can be solved by the finite integral transform technique because the boundary condition at $\eta = 1$ is taken with a constant heat transfer coefficient.

Following the procedure as described in reference [60], the corresponding eigenvalue problem obtained from the homogeneous version of Eq. (19a) is shown in Appendix A. Using the orthogonality of the eigenfunctions, the appropriate transform pair can be written as follows

Transform:
$$\overline{G}_m = \int_{\eta=0}^{1} \eta^i \frac{v(\eta)}{2} G \psi_m(\eta) d\eta \tag{B1}$$

Inversion:
$$G = \sum_{m=1}^{\infty} \psi_m(\eta) \overline{G}_m \tag{B2}$$

Equation (19a) is now multiplied by $\eta^i \psi_m(\eta)$ and integrated from $\eta = 0$ to $\eta = 1$ to obtain,

$$\int_{\eta=0}^{1} \eta^i \frac{v(\eta)}{2} \psi_m(\eta) \frac{\partial G}{\partial \xi} d\eta = \int_{\eta=0}^{1} \psi_m(\eta) \frac{\partial}{\partial \eta} \left[\eta^i g(\eta) \frac{\partial G}{\partial \eta} \right] d\eta + \int_{\eta=0}^{1} \eta^i \psi_m(\eta) \delta^i(\eta - \eta_o) \delta(\xi - \xi_o) d\eta \tag{B3}$$

The first integral in Eq. (B3) is easily evaluated through an application of Liebnitz' rule for the differentiation of integrals and the integral transform (B1). The second integral is integrated by parts twice, making use of boundary conditions (19b,c) and ((A1)b,c) and the

differential Eq. (Ala) and the integral transform (B1). The third integral is easily evaluated with the definition of the delta function. The result is the following infinite set of first order, ordinary differential equations,

$$\frac{d\bar{G}_m}{d\xi} + \lambda_m^2 \bar{G}_m = \psi_m(\eta_o)\delta(\xi-\xi_o) \tag{B4a}$$

with the initial condition

$$\bar{G}_m = 0 \quad , \quad \xi < \xi_o \tag{B4b}$$

Equation (B4a) is integrated with the use of the integrating factor, $e^{\lambda_m^2 \xi}$, to obtain,

$$\bar{G}_m = \psi_m(\eta_o) e^{-\lambda_m^2(\xi - \xi_o)} \tag{B5}$$

The Green's function can now be obtained by substituting the transform $\bar{G}_m$ into the inversion formula (B2). The result is

$$G(\eta,\xi\,|\,\eta_o,\xi_o) = \sum_{m=1}^{\infty} \psi_m(\eta)\psi_m(\eta_o) \exp[-\lambda_m^2(\xi - \xi_o)] \tag{B6}$$

The form of the Green's function needed to construct the kernel of the integral equation (23b) is obtained by evaluating the Green's function (B6) at $\eta = \eta_o = 1$. This gives the following form of the Green's function,

$$G(1,\xi\,|\,1,\xi_o) = \sum_{m=1}^{\infty} \psi_m^2(1) \exp[-\lambda_m^2(\xi - \xi_o)] \tag{B7}$$

The vita has been removed from the scanned document